ELECTROSPUN RECYCLED POLYETHYLENE TEREPHTHALATE MICROFIBERS AS AN ASPHALT MIX ADDITIVE

BY

DEBBRATA DATTA

A thesis submitted in partial fulfillment of the requirements for the

Master of Science

Major in Civil and Environmental Engineering

South Dakota State University

2023

THESIS ACCEPTANCE PAGE
Debbrata Datta

This thesis is approved as a creditable and independent investigation by a candidate for the master's degree and is acceptable for meeting the thesis requirements for this degree. Acceptance of this does not imply that the conclusions reached by the candidate are necessarily the conclusions of the major department.

Rouzbeh Ghabchi
Advisor Date

Nadim Wehbe
Department Head Date

Nicole Lounsbery, PhD
Director, Graduate School Date

This thesis is dedicated

To

My world

(My parents and Siblings).

ACKNOWLEDGEMENTS

First and foremost, I am glad and thankful to God for the blessing that has given upon me in all my endeavors. Secondly, I want to thank my parents and siblings, who have always encouraged me and sacrificed everything to fulfill my dream.

I would like to express my deepest appreciation, sincerest gratitude, and heartiest thanks to my advisor, Dr. Rouzbeh Ghabchi, whose direction and encouragement have been truly inspiring in my academic and professional endeavors. His affectionate and unfailing guidance, constant supervision, energetic encouragement, constructive and helpful criticism, and suggestions at every step throughout the coursework and research assisted me in completing this work. Dr. Ghabchi has been an invaluable help, a source of inspiration, and constant support throughout my journey. He helped me to grow into a researcher and way of thinking. His valuable suggestions and comments helped me to improve my research and writing skills. I am grateful for his mentorship and leadership, which were instrumental in completing this thesis.

I also want to thank my other committee member, Dr. Aritra Banerjee, for offering his time and valuable help in completing this thesis and sharing his knowledge and expertise during my classes with him. I want to thank Dr. Michael Pawlovich for sharing his knowledge and experience with the courses I had with him at South Dakota State University.

I would like to thank Ms. Maryam Mihandoust from the bottom of my heart for her help in my research in every way possible. Her assistance came in various forms: in laboratory testing, answering my questions, and educating me on different aspects of asphalt research and education. Also, I want to offer my special thanks to Mr. Bipin

Adhikari and Mr. Robiul Islam Rubel for their great help and cooperation in completing some research tasks.

I want to express my sincere gratitude to Dr. Muthu Muthukumarappan, Department of Agricultural and Biosystems Engineering, for allowing me to access Raven Precision Agriculture Center. In addition, I would like to sincerely thank Mr. Ken Swedeen with Dakota Asphalt Pavement Association, Mr. Mark Blow with Asphalt Institute, Mr. Noel Schulz and Mr. Leaf Greene with Jebro Inc., Mr. Korey Bender, the President of the Border States Paving, Inc. and Mr. Jason Bowes the President of the Bowes Construction Inc. I also would like to extend my thanks to Jebro Inc., Sioux City, IA., and Concrete Materials Co., Sioux Falls, SD, for generously donating all the materials for this research and for their kind support.

The work presented in this thesis was conducted with support from South Dakota State University and the Mountain-Plains Consortium, a University Transportation Center funded by the U.S. Department of Transportation. The contents of this thesis reflect the views of the author, who is responsible for the facts and accuracy of the information presented.

TABLE OF CONTENTS

ABBREVIATIONS

AASHTO	American Association of State Highway and Transportation Officials
APR	Association of Plastics Recyclers
ASTM	American Society for Testing and Materials
DCM	Dichloromethane
EPM	Electrospun PET Microfiber
FTIR	Fourier-Transform Infrared
HDPE	High-Density Polyethylene
HMA	Hot Mix Asphalt
HVPS	High-Voltage Power Supply
HWT	Hamburg Wheel Tracking
ITS	Indirect Tensile Strength
JMF	Job Mix Formula
LDPE	Low-Density Polyethylene
L-T	Low-Temperature
LVDT	Linear Variable Differential Transformer
MPET	Micronized PET
PET	Polyethylene Terephthalate
SEM	Scanning Electron Microscopy
SGC	Superpave Gyratory Compactor
SHRP	Strategic Highway Research Program
SIP	Stripping Inflection Point
TFA	Trifluoroacetic Acid

TSR	Tensile Strength Ratio
TTA	Templated Transfer Approach
VFA	Voids Filled with Asphalt
VMA	Voids In Mineral Aggregate

LIST OF FIGURES

LIST OF TABLES

ABSTRACT

ELECTROSPUN RECYCLED POLYETHYLENE TEREPHTHALATE MICROFIBERS AS AN ASPHALT MIX ADDITIVE

DEBBRATA DATTA

2023

In recent decades, the use of different types of fibers in asphalt has become increasingly popular. Fibers are used in an asphalt mix to improve its durability and resistance against distresses such as rutting and cracking due to repetitive vehicle loading at high temperatures, and low-temperature contraction. Consequently, accurate rheological and performance characterization of asphalt binders and mixes containing fibers is of vital importance. With increased concerns over the environmental disruptions as a result of disposing end-of-life plastics in landfills and the need for improving sustainability of the construction materials, incorporating plastic in construction materials has always been an important topic for researchers. Among different types of plastics, containers made from polyethylene terephthalate (PET) constitute a large portion of the waste plastic problem. While using waste PET particles in asphalt mixes has been found to be a feasible option, mechanical properties of final product may not adequately benefit from the high modulus and tensile strength of PET plastic. In this study the end-of-life PET plastic obtained from bottled water containers was used for production of PET microfibers using a fiber production technique known as electrospinning. A solution-based electrospinning method was employed in the laboratory to produce electrospun PET microfibers (EPM) by using different concentrations of PET in the solution and discharge rates. Then, the effect of using EPM as an additive on asphalt mix properties was investigated. The selection of PET as the feedstock for EPM production was made due to its high thermal stability, ductility,

surface area, and strain resistance. EPM was produced from a solution of micronized PET (MPET) in a mix of dichloromethane (DCM) and trifluoroacetic acid (TFA). Two MPET concentrations, namely 15 and 20% and various solution discharge rates, namely 40, 50, 60, 120, and 250 µL/min were utilized to determine the effects of the electrospinning parameters on the mechanical and chemical characteristics of the produced EPM. For this purpose, Fourier transform infrared (FTIR) spectroscopy, scanning electron microscopy (SEM), and tensile strength tests were conducted on produced EPMs.

To evaluate the feasibility of incorporating EPM in the asphalt mixes, a comprehensive testing program was carried out in this study. The performance of asphalt mixes containing different amounts of EPM was assessed by conducting Hamburg wheel tracking (HWT), semi-circular bend (SCB), and tensile strength ratio (TSR) tests. These tests were included in the experimental design to determine the resistance of the asphalt mixes to rutting, cracking, and moisture-induced damage.

FTIR spectroscopy analysis revealed that the electrospinning parameters and solution's proportions did not alter the molecular structure of the PET or generate new molecules. Analyzing the SEM micrographs showed that the diameter distribution in the EPM fibers decreased with a reduction in discharge rates at a constant MPET concentrations. In addition, morphological examination of SEM micrographs suggested that the most uniform and smooth fibers were consistently produced at the lowest discharge rate. Increasing the discharge rates resulted in the formation of fibers with rough textures, non-uniform in shape and size, and fractured. The mechanical properties of the produced EPM also exhibited a correlation with the fibers' diameters. More specifically, fibers having smaller diameter resulted in enhanced mechanical properties. In view of the

findings pertinent to the EPM's chemical composition, morphological characteristics, mechanical properties, and yield consideration electrospinning using a solution of 20% MPET concentration and a discharge rate of 60 µL/min was found to result in EPMs of optimal mechanical and morphological properties.

Performance tests conducted on asphalt mixes revealed that the addition of EPM to asphalt mixes improved their resistance to rutting, based on the HWT test. Asphalt mixes containing 0.5 and 1.0% EPM by binder weight tested in a HWT device exhibited a resistance to rutting and moisture-induced damage which were greater than those of the mixes which did not contain any EPM. However, increasing the EPM content to 1.5% by the weight of binder was not found to benefit its resistance to rutting. Conducting TSR tests on asphalt mixes revealed that incorporating EPM in the mixes enhanced their resistance to moisture-induced damage, confirming the findings of the HWT tests. Finally, conducting SCB tests revealed that incorporating EPM in asphalt mixes resulted in an improved resistance to cracking when compared to mixes which did not contain any EPM. Overall, it was concluded that incorporating EPM in asphalt mixes can potentially be a feasible approach to reduce plastic landfills and improve the performance and sustainability of the ground transportation system.

CHAPTER ONE: INTRODUCTION

1.1. Background

Hot mix asphalt (HMA) is a composite material consisting of aggregates and asphalt binder primarily used to build roads and airport pavements. More than 90 percent of highways and paved roads in the United States are constructed with asphalt. In addition, according to the National Asphalt Pavement Association (NAPA), the United States produces approximately 500 million tons of new asphalt mix annually. Asphalt pavements may experience different distresses such as rutting (permanent deformation), raveling, fatigue cracks, moisture-induced damage, and low-temperature (L-T) cracks (Copeland, 2011) among other distresses. Consequently, to improve the quality and durability of the asphalt pavements, the pavement industry is continually researching materials and methods to enhance the engineering properties of asphalt binder and asphalt mix. For example, incorporating different types of additives such as polymers, fibers, adhesion boosters, and asphalt recycling agents into the HMA is known as an effective method to improve the engineering properties of asphalt binders and mixes. Various types of polymer and fibers used in asphalt binder as additives are capable of increasing the resistance of asphalt pavements to rutting and cracking, extending their service life. For example, previous studies have reported that incorporating fibers in asphalt mixes prevent asphalt binder bleeding (Serfass and Samanos, 1996; Hassan et al., 2005). Other studies also suggested that the addition of fiber to asphalt mix modifies its viscoelastic properties (Peltonen, 1991a; Huang and White, 1996), resulting in an enhanced creep compliance and resistance to rutting (McDaniel, 2001; Putman and Amirkhanian, 2004), and an improved resistance

to moisture-induced damage (Wu et al., 2008). It has also been reported that incorporating fibers in asphalt mixes resulted in a reduction in reflective cracks when compared with mixes which did not contain fibers in them (Chen et al., 2004; Tapkin, 2008). Other studies have found that fibers in asphalt mixes can help improve their resistance to low temperature cracks, fatigue cracks, and overall enhanced durability (Huang, 2004; McDaniel, 2001; Maurer and Malasheskie, 1989; Lee et al., 2005; Freeman et al., 1989). Furthermore, several other properties of asphalt mixes, including wear resistance (Hassan et al., 2005), toughness, tensile strength (Wiljanen, 2003; Chen et al., 2005), dynamic modulus (Wu et al., 2007), and elasticity (Peltonen, 1991b), are reported to improve as a result of inclusion of fibers in HMA. However, the addition of fiber may result in increased air voids within the HMA, necessitating additional compaction efforts to attain the same density compared to the HMA without fiber (Peltonen, 1991a). Two methods are used to incorporate fibers in HMA: modification of the asphalt binder (terminal blending) and addition of fibers to asphalt mix (plant mixing). Currently, a variety of fibers, including lignin, basalt, and polyester fibers are successfully incorporated in asphalt (Xiong et al., 2015). In the present study, PET microfibers produced from waste PET by applying the solvent-based electrospinning technique was used. The selection of the PET fibers for this study was made based on its superior mechanical properties as well as significant environmental advantages its recycling will result. A number of factors contributing to the use of PET for producing EPM are summarized as follows.

PET with its high melting point, thermal stability, tensile strength, stiffness, and chemical resistance (Dhaka et al., 2022; Ben Zair et al., 2021; Miao et al., 2021; and Ma et al., 2018) is widely utilized for various applications including protective gear, membranes,

vascular grafts, tissue scaffolding, filtration (Strain et al., 2015) and beverage industries (Zander et al., 2016). But, single-use PET plastics, such as beverage bottles, are frequently discarded in the environment, leading to serious environmental concerns (Koo et al., 2014). For example, researchers observed that as a form of microplastics, PET can enter food chain and consumption of those microplastics can result in decreasing in the migration and proliferation of human mesenchymal stem cells in bone marrow and endothelial progenitor cells (Dhaka et al., 2022). To mitigate the PET waste problem, research on the natural decomposition of those plastics is going on using specific bacterial micro-organisms (Vo et al., 2018). Despite ongoing efforts, PET is still considered a non-biodegradable material (Ben Zair et al., 2021). In addition, disposal of PET in landfills or burning in open air poses significant environmental challenges and health risks (Chavan and Rao, 2016). Due to its single-use nature (Vo et al., 2018) and increase in production of PET bottles year by year (NAPCOR, 2019) recycling and repurposing this stream of plastic waste should become an environmental and economic priority. Therefore, incorporating PET fiber in asphalt pavement can be a sustainable avenue for management of waste PET. However, before this can be achieved, it is important to explore the feasibility of using different forms of PET plastic in asphalt mixes.

Some studies suggested that the addition of PET to asphalt mixes has the potential to improve its overall performance. Researchers have incorporated recycled PET in asphalt mixes in two forms: as crushed PET (aggregate replacement), or as chemically procced PET. For example, different studies have recycled PET as a synthetic aggregate in asphalt mixes. However, it was not reported that the use of PET aggregates significantly enhanced the performance of mixes when compared to those which did not contain PET aggregates

in them (Hassani et al., 2005; Ahmadinia et al., 2012; Moghaddam et al., 2012; Modarres and Hamedi, 2014a;2014b). Other studies in which micronized PET (MPET) was used as an asphalt binder modifier have reported an improved resistance to rutting and cracking as compared with those which did not contain any MPET (Ghabchi et al., 2021; Silva et al., 2018).

Findings from those investigations also suggested that a couple of challenges associated with the storage stability issues of PET-modified binders, the thermal incompatibility of micronized PET with asphalt mix, and the inefficiency of the milling process used to produce micronized PET are main obstacles to recycling PET as MPET in HMA. Therefore, to overcome those challenges, different studies had been proposed by Merkel et al., (2020); Leng et al., (2018a, b) using chemical processing of PET to incorporate it into asphalt mixes as an alternative method. According to those studies, the use of chemically processed PET-modified asphalt binder can enhance resistance to rutting, fatigue cracks, and low-temperature cracks in comparison to unmodified asphalt binder. Despite promising results, there are still concerns regarding using chemically processed PET in HMA because of the energy required for the chemical reaction, the need for multiple chemicals, and the production of toxic byproducts (Merkel et al., 2020) as all contribute to an increase in construction cost and environmental impact. Therefore, the purpose of this study is to address these environmental issues associated with recycling PET waste and to overcome the obstacles associated with the existing recycling techniques used to incorporate PET into asphalt mixes. In addition, this study also covers the area of integrating PET into the load-bearing structure of asphalt mixes to capitalize on PET's superior mechanical properties. To accomplish these objectives, microfibers from waste

PET bottles by applying electrospinning techniques in the laboratory were used.

Laboratory production of electrospun PET microfiber (EPM) was conducted to resolve environmental concerns associated with PET waste and to increase the performance of asphalt mixes. The structure and morphology of EPM were analyzed using imaging techniques. Using laboratory-prepared HMA specimens, the resistance of EPM-modified asphalt mixes to cracking, rutting, and moisture-induced damage were also evaluated.

1.2. Research Objectives

The specific objectives of this study are as follows.

a) Produce PET microfibers in the laboratory through the application of solvent-based electrospinning technique by using MPET as feedstock.

b) Determine the effect of electrospinning parameters, namely PET concentration and discharge rate on the mechanical, morphology, and chemical properties of the electrospun PET microfibers (EPM). Characterize the tensile strength, morphology, and chemical structure of the produced EPM by conducting tensile strength tests and applying scanning electron microscopy (SEM) and Fourier-transform infrared (FTIR) spectroscopy.

c) Characterize the effect of using EPM on the resistance of asphalt mixes to cracking, rutting, and moisture-induced damage by conducting semicircular bend (SCB), Hamburg wheel tracking (HWT), and tensile strength ratio (TSR) tests, respectively.

1.3. Significance of the Study

The present study was conducted to determine the viability of using EPM generated from waste PET as a modifier to improve the mechanical properties of asphalt mixes. This investigation will have a positive effect on the environment by reducing the amount of PET bottles that end up in landfills. It is also expected to reduce the need for costly polymers derived from petroleum, which are commonly used to modify asphalt binders.

The use of asphalt mixes modified with EPM is anticipated to result in pavements that are more resistant to cracking, rutting and more durable than those without EPM. This will extend the life of the pavement and reduce the need for polymer-modified asphalt compounds, resulting in reduced construction and maintenance costs. In addition, the results of the study will assist pavement engineers in comprehending the impact of EPM on HMA mix formulations. Consequently, the proposed study is anticipated to have substantial economic and environmental benefits. The benefits of this research are expected to support environment preservation and the sustainability of the ground transportation system, an important step toward a sustainable infrastructure.

1.4. Plan of Study

Specific tasks to be carried out in the study are as follows.

a) Prepare a solution by adding dichloromethane (DCM) and trifluoroacetic acid (TFA) at a ratio of 30:70 (volume/volume) and mixing the solvent with two different amounts of ground PET (15 and 20%) to produce EPM.
b) Produce EPM utilizing previously prepared solutions and different solution discharge rates using the static electrospinning technique.

c) Characterize the tensile strength, morphology, and chemical structure of the produced EPM by conducting tensile strength test and applying SEM and FTIR spectroscopy.

d) Optimize discharge rate and ground PET percentage for the mass productions of fibers based on produced fibers' characteristics and observations made during the of production EPM by electrospinning technique.

e) Collect the asphalt binder, namely PG 58-28 and determine the optimum binder content of asphalt mixes using volumetric mix design for a given aggregate structure.

f) Prepare asphalt mixes using optimum binder content and various percentages of EPM.

g) Determine the effect of EPM contents incorporated in HMA mixes on their resistance to rutting, cracking, and moisture-induced damage in accordance with AASHTO T 324 (AASHTO, 2011), ASTM D8044 (ASTM, 2017), and AASHTO T 283 (AASHTO, 2011) standard methods, respectively.

Thesis Organization

This thesis is arranged and presented in the following order:

Chapter 1: Introduction – The background section of this chapter provides general information about asphalt binders and HMA. Besides, the benefits of adding different additives in binders and HMA such as fibers are discussed. Following the background, the research objectives, significance of the study, plan of study and thesis organization are presented.

Chapter 2: Literature Review – This chapter is divided into three parts. The first part is a summary of the literature review, which focuses on the production, usage, problems associated with plastics and their possible uses in different fields of engineering. The second part provides a review of previous studies related to rheological and mechanical properties of polymer, fiber, and non-modified binders. In addition, limitations of conventional binder characterization methods are discussed. This chapter also provides a summary of previous studies related to the characterization methods for asphalt mix, and their respective limitations.

Chapter 3: Materials and Methods – This chapter describes the details of the material selection and collection, and production of EPM, and asphalt mixes. In addition, the laboratory testing procedures and test matrix used to evaluate the produced EPM, as well as EPM-modified asphalt mixes, are discussed. In this chapter, various test methods, such as SCB, TSR and HWT tests, among others, are presented.

Chapter 4: Test Results of PET Fibers – Mechanical, morphological, and chemical properties of the produced PET fibers produced using different electrospinning parameters are presented in this chapter. More specifically, EPMs' roughness, entanglement, average diameter, and tensile strength are summarized and discussed in this chapter.

Chapter 5: Test Results of Asphalt Mixes – The results of HWT, SCB, and TSR tests conducted on asphalt mixes containing different amounts of EPM are presented and discussed in this chapter.

Chapter 6: Conclusions and Recommendations– This chapter presents the study's key findings. In addition, suggestions and recommendations for implementation and future research are included in this chapter.

CHAPTER TWO: LITERATURE REVIEW

2.1. Background

Plastics are widely used as an essential part of almost every aspect of our daily life. The plastic industry has grown tremendously since the development of numerous methods for producing polymers from petrochemical sources. It has substantial advantages over many other materials in terms of its low weight, toughness, and lower price (Dhaka et al., 2022; Ben Zair et al., 2021; Ghabchi et al., 2021; Hopewell et al., 2009). Among different types of plastic, PET is widely utilized for various applications including protective gear, membranes, vascular grafts, tissue scaffolding, filtration (Strain et al., 2015) and beverage industries (Zander et al., 2016). To mitigate the end-of-life plastic problem and proper waste management, engineers, and researchers are trying to introduce waste PET into pavement industry through applying different techniques. This chapter will discuss possible challenges, techniques, and performance of PET-modified asphalt.

2.2. Availability of Waste PET Plastic

At a compound annual growth rate (CAGR) of 10.6 percent, the size of the global PET market is expected to increase from $35.47 billion in 2021 to $39.23 billion in 2022, and then to $57.19 billion in 2026 with a CAGR of 9.9 percent. This fact indicates that an increasing number of PET will be available in the global market in the near future (Fortune Business Insights, 2022). Additionally, a report published by the national association for PET container resources (NAPCOR) indicated that in 2018, US market sold about 6,270 million pounds of PET bottles, but only 1,816 million pounds, or about 29.0 percent, were

collected and resold through recycling programs. That means around 71 percent of PET bottles were left to the environment and waiting for recycling or landfilling. This amount is produced in only one year and each year it is increasing.

In addition, the association of plastics recyclers (APR) provided a detailed summary of the United States National Postconsumer Plastic Bottle Recycling Report (NAPCOR, 2019) and concluded that PET and high-density polyethylene (HDPE) bottles comprise 97.1 percent of the United States plastic bottle market, and the rest of them are polypropylene (PP), low-density polyethylene (LDPE), and polyvinyl chloride (PVC). Although 98.9 percent of recycled plastics are either PET or HDPE, still the last destination of large amounts of plastics is either ending up in landfills or left in the environment.

Consequently, environmental pollution and toxicity of the waste PET have become a significant concern as those debris have been found in groundwater, drinking water, soil, and the ocean (Smith et al., 2022). Researchers also discovered that PET in the form of microplastics can infiltrate food chains, a reason for concern as plastic ingested by humans can cause diseases, such as a reduction in the migration and proliferation of human mesenchymal stem cells in bone marrow and endothelial progenitor cells (Dhaka et al., 2022). Therefore, the widespread generation of waste PET needs a proper end-of-life management solution (Sulyman et al., 2016).

2.3. Responsible and Sustainable Recycling of PET

Waste PET bottles are primarily recycled by either a mechanical or chemical processes (Ben Zair et al., 2021; Khoonkari et al., 2015). This process involves the grinding of PET water bottles into flakes (NAPCOR, 2018). For instance, in 2019, 806 kilotons of recycled PET flakes were produced from 2,887 kilotons of post-consumer PET in the

United States to manufacture recycled products such as fibers, sheets and films, strapping, and food and beverage bottles, among other products. These efforts accounted for 27.9% of total PET consumptions (NAPCOR, 2019). Due to the technical challenges associated with reusing waste PET, its recycling rates are still low. Those challenges mainly consist of collection, sorting, reclaiming, and converting processes (Smith et al., 2022; Leng et al., 2018a). In addition, stable and low cost of virgin PET does not offer economic incentives for recycling (Vo et al., 2018). To generate value-added products from waste PET, it can be synthesized into nanofibers with high surface-to-volume ratio and porosity, which can replace virgin PET in highly valued applications such as batteries (Jung et al., 2016), sensors (Senthamizhan et al., 2014), tissue engineering (Santoro et al., 2016), pharmaceutical industry (Hu et al., 2014), and filter media (Bonfim et al., 2021). Many studies have been carried out to investigate the manufacturing of micro and nano fibers from PET plastics. Strain et al. (2015), for instance, synthesized nanofibrous isotropic membranes from recycled PET using 30:70 weight ratio of DCM and TFA solutions and then produced PET mat for air filtration applications. Therefore, producing nano or microfibers from MPET can be a sustainable method of application-based recycling.

2.4. Electrospinning: A Promising Technique for Fiber Production

Among nanofiber production techniques, electrospinning, one of the most rapidly growing commercial polymer processing methods, is widely used for the manufacturing ultrathin nanofibers and nonwoven membranes (Huang et al., 2003). Electrospinning can be accomplished using two distinct approaches: melting-based electrospinning and solution-based electrospinning (Dasdemir et al., 2013). In melting-based electrospinning significant amounts of heat are required to melt the material, and repeated heating cycles

degrade the material's mechanical properties (Beyler and Hirschler, 2002; Spinacé and De Paoli, 2001). Another drawback of this process is that high viscosity of molten polymers makes it difficult to manufacture very thin, uniform fibers (Thompson et al., 2007). For this reason, solvent-based electrospinning as an alternative approach is used as it provides a high-quality control over fiber morphology (Strain et al., 2015). In this approach, fibers are generated by applying an electric field to a polymer solution between two electrodes with opposite charges, one of which is coupled to the syringe containing the polymer solution and the other attached to a conductive collector. When electrostatic force overcomes the surface tension of a fiber-forming solution, electrospinning occurs and a Taylor cone forms from solution droplets (Owida et al., 2022; Christiansen et al., 2021; Koenig et al., 2019**;** Xu et al., 2017; Zander et al., 2016; Huang et al., 2003; Doshi and Reneker, 1995). Also, in solution-based electrospinning, fiber morphology, geometry, and production rate are all influenced by various processing parameters, such as applied voltage, flow rate, nozzle diameter, collection distance, solution properties (including polymer molecular weight, concentration, electrical conductivity, surface tension, and solvent properties) as well as ambient conditions like temperature and humidity (Fang and Lin, 2019; Cramariuc et al., 2013; Tan et al., 2005).

2.5. Characterizations of PET Fibers

Tensile strength, elongation, Young's modulus, and Poisson’s ratio are important mechanical properties of EPM. Zhang et al. (2011) used ASTM D882 standard procedure (ASTM, 2018) to prepare fiber specimens of 7 mm width and 15 mm length, and a crosshead with displacement rate of 30 mm/min to conduct stress-strain analysis at room temperature. Strain et al. (2015), on the other hand, employed a templated transfer approach

(TTA) to determine the tensile strength of fibers. Tensile strength was calculated as the highest stress supported during the test, Young's modulus as the initial linear slope of the stress-strain curve, and toughness as the total area under the stress-strain curve. Vo et al. (2018) tested fiber samples with a universal tensile testing machine (gauge length: 20 mm, crosshead speed: 0.5 mm/s) at 20°C and 30% relative humidity (RH). Kim et al. (2011) used ASTM D3822 (ASTM, 2007) to determine tenacity, elongation at the failure point, and young's modulus of single fibers.

The FTIR spectrometer was utilized by researchers to understand the chemical composition of different plastics. Using FTIR with a wavenumber range of 4,000 to 400 cm^{-1}, the functional groups of produced PET fiber mats can be determined (Abbas et al., 2018; Espíndola-González et al., 2011). Determining the morphological properties of a fiber mat, such as fiber diameter and orientation, is a difficult process for which no well-established method exists. SEM is widely used for the morphological analysis of the electron spun fibers (e.g**.,** Vo et al., 2018**;** Xu et al., 2017; He et al., 2015; Wang et al.,2013; Li et al., 2012; Ogata et al., 2007). SEM analysis does not directly provide the diameter of the fiber, instead, it will produce a scanned image of the fiber mat. Therefore, using digital pictures generated by SEM equipment, the researcher uses a variety of approaches to measure the diameter. For example, the fiber's mean diameter was determined using AutoCAD® software from an SEM image (Xu et al., 2017; Wang et al.,2015). Vo et al. (2018) employed image processing software (ImageJ) to estimate the diameters of fibers at a magnification of 2000x. They also used Origin software to compute the size distributions of the measured fibers. Li et al. (2012) used Smile View software to analyze SEM images and determined the average fiber diameter. Besides, Zhang and Seeger (2011)

suggested a micrometer for the determination of fiber diameter. Additionally, the researchers employed a digital magnifier to measure various parameters linked to digital images of fibers. For example, Li et al. (2012) used energy dispersion spectroscopy for chemical analysis while conducting the SEM test.

Crystal orientation in the fiber bundle is also one of the important parameters affecting the mechanical properties of the produced fibers. Ogata et al. (2007**)** employed a spinning disk with a circumferential speed of approximately 1 mm/min, to produce unidirectionally aligned PET fibers. He et al. (2015) utilized polarized FTIR spectroscopy to examine the crystal orientation of fibers in the amorphous regions. Other researchers used a differential scanning calorimeter (DSC) with a heating scan rate of 10°C/min in a temperature ranging from ambient temperature to 300°C in nitrogen to gain an understanding of thermal properties of the fibers (Vo et al., 2018; He et al., 2015; Strain et al., 2015; Wang et al., 2015; Li et al., 2012; Ogata et al., 2007). DSC thermograms, on the other hand, were processed and obtained during the first heating of the fiber sample in the temperature range of 30 to 300°C at a rate of 20°C/min (Kim et al., 2011).

2.6. Distresses in Asphalt Pavement

Various types of distresses such as rutting, fatigue cracking, and thermal cracking, are visible in asphalt pavement which can affect the pavements performance. Particularly, freeze-thaw cycles, low temperature, and permanent deformation (rutting) can have negative effects on the performance of a pavement. These distresses can be caused by a combination of factors, including environmental conditions, construction issues, and the repeated passage of vehicles with high axle loads (Chen and Xu, 2010; Xu and Solaimanian, 2008; Liu et al., 2014).

Rutting is the surface deformation along the wheel path caused by traffic loads, especially during summer when the binder viscosity is reduced due to high pavement temperatures. In contrast, fatigue cracking is caused by traffic loads at intermediate temperature and characterized in its early stages by longitudinal cracks on the wheel path, which later develop into alligator cracking. The main cause of fatigue cracking is the application of loading cycles caused by traffic. On the other hand, thermal cracking happens due to extreme variations in ambient temperature from high to low, resulting in uniformly spaced transverse cracks (Behnood and Gharehveran, 2019). These distresses can lead to an increase in maintenance costs and negatively affect pavement's overall performance and life span (Yu et al., 2009).

2.6.1. Rutting in Asphalt Mix

Asphalt mix is a heterogenous material consisting of air, binder, and aggregates which is frequently used in the construction of modern pavements (Huang et al., 2003). During asphalt pavement's service life, it may be subjected to various forms of distress such as rutting. Rutting is one of the most common and significant distresses, and it can occur in both asphalt and underlying unbound layers. It is considered one of the primary modes of pavement distress and can have a significant impact on the pavement’s performance and durability (Domingos and Faxina, 2016; Norouzi et al., 2016; Faruk et al., 2015; Shukla and Das, 2008). Approximately, between 85 and 95% of rutting occurs in asphalt pavement layer where water infiltrates into pavement layers (Coleri et al., 2008). It is characterized by a depression in the surface that develops along the wheel paths. Rutting is typically the result of a combination of densification and shear deformation,

which causes longitudinal depressions and small upheavals along the wheel paths (Du et al., 2018 and Simpson, 1999).

The HWT test is widely utilized to evaluate the resistance of asphalt mixes to rutting. This test is especially useful for identifying premature failure of HMA mixes due to insufficient binder rigidity, poor aggregate packing, susceptibility to moisture damage, and insufficient aggregate-binder adhesion. Thus, the HWT test provides valuable insights into the performance of asphalt mixes under various conditions, enabling the optimization of pavement design and maintenance strategies (Chaturabong and Bahia, 2017). Since the early 1990s, this method has been extensively used to evaluate the rutting resistance and moisture susceptibility of asphalt mixes. Permanent strain or rutting depth versus loading cycle (Figure 2.1) obtained from conducting HWT test can be divided into three distinct phases: a) the post-compaction phase, b) the creep phase, and c) the stripping or damage phase. Each of these phases provide crucial information about the asphalt mixture's behavior under various conditions, enabling engineers to make decisions regarding the design and maintenance of pavements (Hoffman and Solaimanian, 2019).

A total rut depth from HWT test can provide an idea of rutting resistance. The stripping inflection point (SIP) (Figure 2.2) in the HWT graph indicates the point where asphalt binder begins to separate from the aggregates (Solaimanian et al., 2003). However, these two parameters may not adequately capture the complex mechanisms underlying rutting and moisture susceptibility. This is since rutting can result from both water damage and continuous deformation due to repeated loading (Aschenbrener and Currier, 1993).

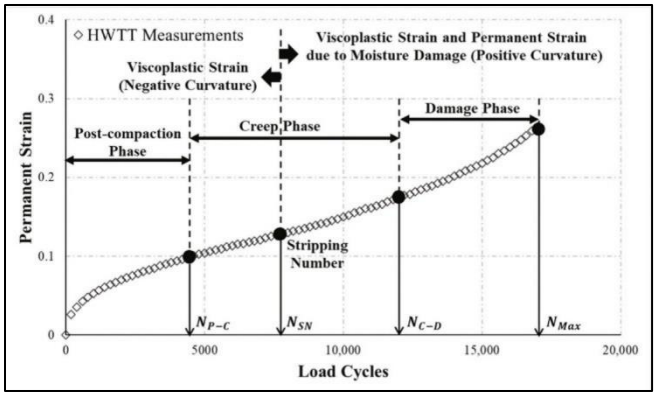

Figure 2.1 Load cycles-deformation curve from testing asphalt sample in HWT (after Zhang et al., 2021)

Consequently, at a given number of load cycles, when an SIP occurs, rut depth cannot be utilized effectively to assess the resistance of the mix to rutting (Park et al., 2017) as specimen may reach to failure point governed by both moisture damage and rutting (Schram and Williams, 2014; Ghabchi and Acharya, 2022).

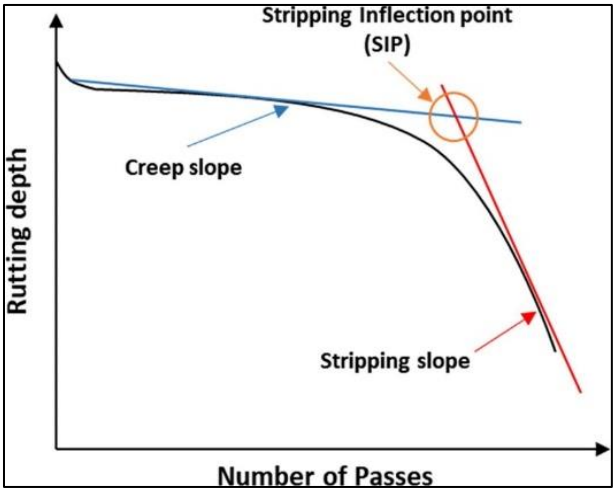

Figure 2.2 Stripping inflection point (SIP) (after Moon et al., 2022)

2.6.2. Cracking in Asphalt Mix

The term, fatigue failure of asphalt mixes, defines structural failure under repeated traffic load which is a gradual process in which small fractures accumulate and expand over time (Cong et al., 2017). Maltenes, a non-polar component of binders, are responsible for forming large networks inside the asphalt mixes (Sperling, 2005). These networks'

mechanical behavior is determined by the elongation and warping of intermolecular bonds and thus it also determines the brittleness of mixture as well. Since plastic deformations are limited to the binder's brittleness, after each load cycle, energy is dissipated through fatigue damage (Rosen, 1964). As binders' stress-strain behavior is affected by temperature, it plays a crucial role in determining the mechanical resistance of asphalt mixes to fatigue damage as well (Moreno-Navarro et al., 2018). Measuring fracture energy can provide insightful information regarding the efficacy of asphalt mixes under repeated loading. Numerous methods have been developed for determining fracture energy and rank fracture toughness but a majority of them were originally devised for core-based specimens and some of them have been adapted from other disciplines. Chevron bend specimen and the short rod specimen are commonly used to measure fracture energy in rocks and other materials. With some modifications, those techniques were adopted to be applied for characterizing asphalt mixes (Ouchterlony, 1990). Several researchers have examined the fracture properties of asphalt specimens at intermediate temperatures to differentiate the resistance of various materials to cracking.

In the 1990s, the semicircular bend (SCB) test was applied to determine the resistance to cracking and the rate of fracture propagation in asphalt mixes. The SCB test is considered to be more accessible than other methods, such as those introduced by Chong and Kuruppu, (1984), due to its simplicity and low cost. The SCB test acquired popularity in the early 2000s due to its uncomplicated specimen preparation process using the SuperPave gyratory compactor (SGC) or by core collected from the field, and relatively simple testing procedure (Hofman et al., 2003). Recently, researchers have examined the fracture resistance at intermediate temperatures of various asphalt mixes using the SCB

test (Al-Qadi et al., 2015; Huang et al., 2013; Mohammad et al., 2012; Nsengiyumva et al., 2015). Figure 2.3 presents the SCB setup.

Figure 2.3 SCB sample setting in the machine

Mull et al. (2002) examined the applicability of the SCB sample by determining a fracture parameter known as critical strain energy release rate (J_c) using Equation 2.1:

$$Jc = -\left(\frac{1}{b}\right)\frac{dU}{da} \tag{2.1}$$

where J_c = critical strain energy release rate (kJ/m^2), b = sample thickness (m), a = notch depth (m) and U = strain energy to failure (N.m).

2.6.3. Moisture Damage in Asphalt Mix

Moisture damage is one of the primary distresses leading to premature failure in pavements as it can severely compromise their strength and overall service life (Brekah and Williams, 2015; Sengoz and Agar, 2007). Due to moisture damage, only in 2005, highway agencies in the United States invested an additional $54 billion in maintenance costs (Copeland, 2005).

Moisture damage also referred to as stripping, can be accelerated due to

environmental conditions, production and construction practices, pavement design, and traffic volume, and material properties (Mercado, 2007). Pavement striping **(**Figure 2.4**)** can be mitigated by judicious material selection strategies (Bagampadde et al., 2006). Different mechanisms of adhesion and debonding between asphalt binder and aggregate are responsible for moisture damage. Most of the mechanisms are based on physio-chemical interactions between the asphalt binder and aggregate, categorized as mechanical adhesion, physical adhesion, and chemical bonding and debonding (Bhasin, 2007). Researchers believe that moisture damage is the progressive degradation of pavement performance caused by the collapse of adhesion bonds (Figure 2.4b) at the interface of aggregate and mastic or the loss of cohesion (Figure 2.4b) within the mastic because of moisture (Kiggundu and Robert, 1988; Bozorgzad et al., 2018a). Environmental conditions such as high relative humidity, intense precipitation, and freeze-thaw cycles can accelerate moisture damage (Bozorgzad et al., 2018b).

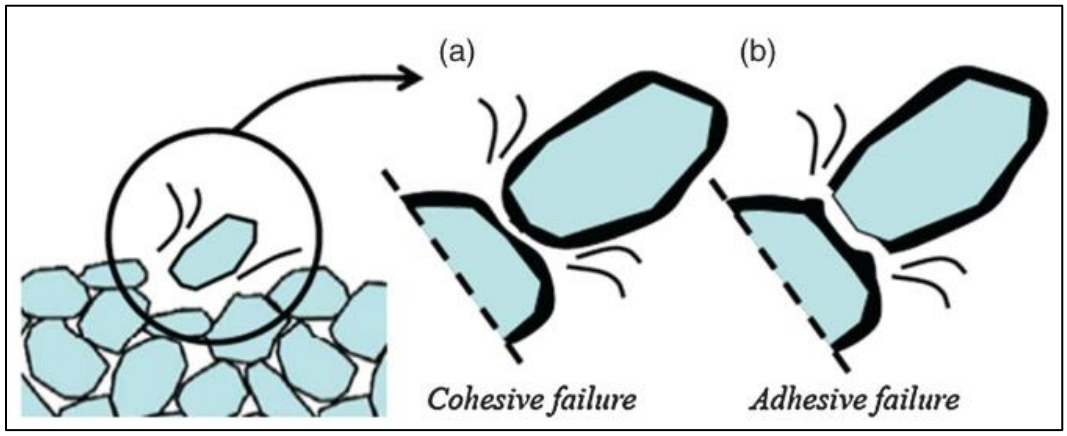

Figure 2.4 Stripping due to (a) cohesive; and (b) adhesive failures in the asphalt mix (after Kringos, 2007)

Premature deterioration of pavement can get even worse due to aging of the asphalt mixes. Short-term aging occurs during the production of the mix and the construction of the pavement, while long-term aging occurs during the pavement's service life. The aging

of asphalt mixes as a result of oxidation and exposure to solar ultraviolet radiation increases the brittleness of asphalt mix and weakens binder-aggregate adhesion specifically in areas near to the surface. Moisture damage becomes increasingly severe as both air and water predominantly move through interconnected air voids in asphalt pavements. When evaluating the moisture susceptibility of asphalt mixes, it is essential to consider the effects of aging (Das et al., 2015). Various methods, including the tensile strength ratio (TSR), binder bond strength (BBS), and Duriez tests are utilized to evaluate the moisture resistance of asphalt mixes (Solaimanian, et al., 2003). Based on empirical observations, these methodologies provide a moisture index ratio that reflects the specimen's retained resistance after conditioning.

2.7. Asphalt Mix Modification Using Different Types of Fibers

Various additives can be incorporated as modifier into asphalt mixes to reduce pavement distress mentioned in section 2.6. and improve pavement performance. These modifications are intended to mitigate or delay emergence of the previously mentioned types of pavement distresses (Oruc et al., 2022).

Fibers are added to improve the mechanical properties of conventional dense graded asphalt mixes (Kumbargeri and Biligiri, 2016; Großegger, 2016)**.** The incorporation of fiber-reinforced asphalt materials in pavement construction is shown to enhance resistance to rutting, fatigue cracking, and moisture-induced damage (Goel and Das, 2004). In fiber-reinforced asphalt some portion of traffic-induced shear and tensile stresses in asphalt mix is transferred to the fiber, improving resistance of the asphalt mix to rutting and cracking. This performance benefits depend on the type, mechanical properties, shape, length, thickness and amount of the fibers incorporated in the asphalt mix (Ali et al., 2020;

Park et al., 2015). However, addition of fibers can result in the increase of binder stiffness which may lead to brittleness in pavement and other distress (Chen and Lin, 2005).

Furthermore, fibers can be used to prevent binder bleeding for mixes with high binder content (Shukry et al., 2016; Großegger, 2016). In addition, fibers in asphalt reduce air voids by impeding water flow through interconnected voids (Marchioni and Becciu, 2015). There are numerous varieties of fibers, including polypropylene, polyester, asbestos, cellulose, carbon, steel, glass, and nylon fibers, each of which possesses its own distinct material properties. These fibers have been utilized in asphalt mixes in various ways to improve their performance (Nelson et al., 2002; Ye et al., 2009; Abtahi et al., 2010). The efficacy of various types of fibers in pavement applications are summarized in following sections.

2.7.1. Cellulose Fibers

Cellulose fibers produced from the bark, wood, or leaves of plants have greater surface area than mineral or polyester fibers and a higher ability to bond with binder (Chen and Lin, 2005). According to a study conducted by Ye and Jian (2019), adding 0.3 to 0.5% cellulose fibers to an open graded friction course (OGFC) better enhanced the binder's stability in comparison to polypropylene and polyester fibers. In addition, Afonso et al. (2017) discovered that, due to their high binder absorption capacity, cellulose fibers increase the rutting resistance of HMA, but not the raveling resistance when combined with neat binders. In addition, the incorporation of cellulose fibers resulted in an increase in particle loss when tested using Cantabro method in wet condition, Valeri et al. (2018) reported that cellulose fibers enhance raveling resistance up to a certain fiber content, beyond which raveling resistance begins to drop. As the fiber content exceeds the optimum

binder content, the cohesiveness of the binder decreases, resulting in particle loss. However, when combined with modified binders, cellulose fibers can increase asphalt mixes' resistance to raveling.

2.7.2. Mineral and Glass Fibers

Mineral fibers are rigid and have the lowest softening point compared to polyester and cellulose fibers. Up to a certain optimal fiber concentration, the complex modulus of asphalt mixes with mineral fibers increases which results in increased stiffness and resistance to rutting. Beyond the optimum fiber content (OFC), complex modulus of asphalt mixes decreases (Chen and Lin, 2005).

Mineral fibers are effective at decreasing binder bleeding (Ma et al., 2018; Tanzadeh et al., 2019), but in aged and unaged Cantabro test, their efficacy is not found to be adequate. Glass fibers, on the other hand, can enhance Indirect tensile strength (ITS) (Tanzadeh and Shahrezagamasaei, 2017; Chen and Lin, 2005), whereas the addition of mineral fibers decreases resistance to moisture damage (Tanzadeh and Shahrezagamasaei, 2017). Due to their high tensile modulus and low thermal susceptibility, glass fibers have been utilized in the textile processing sector (Tanzadeh and Shahrezagamasaei, 2017). The addition of glass fibers to asphalt mixes significantly increases their ITS value (Tanzadeh and Shahrezagamasaei, 2017; Tanzadeh et al., 2019; Enieb et al., 2021) and binder absorption, resulting in an increase in air void and binder content without binder draining (Slebi-Acevedo et al., 2019). According to Wang et al. (2019), glass fibers also improve the cracking resistance of asphalt mixes, especially at low temperatures.

Tanzadeh et al. 2019, reported that the addition of 12-millimeter-long glass fibers improved the mix's stiffness and tensile strength. This study also revealed that the fibers

reduced the permeability of the mixture, which could impact the asphalt pavement ability to drain water. In addition, glass fibers strengthen the asphalt mix's elastic properties by functioning as an elastic medium to improve the mix stiffness. Consequently, glass fibers are a viable option for reducing rut depth in mixes (Enieb et al., 2019). The addition of glass fiber to asphalt mixes increases ductility, fatigue life, and high-temperature stability by augmenting the mixture's resistance to rutting (Tanzadeh et al., 2019; Luo et al., 2019).

2.7.3. Steel Fibers

Steel fibers are a form of reinforcement that not only improve the mechanical properties of asphalt mixes, but also possesses self-healing properties **(**Karimi et al., 2018; Phan et al., 2018; Sun et al., 2016; Wang et al., 2016). They can be used in electrothermal procedures to treat asphalt mix. The samples when subjected to an electromagnetic field, can produce heat as a result of generating currents in the conductive steel fibers. Consequently, the binder melts and fills the micro fractures, preventing further crack propagation, a process known as self-healing **(**Liu et al., 2010). Additionally, the incorporation of steel fibers significantly enhances the resistance to particle loss (Lastra-González et al., 2020). Besides, according to Lastra-Gonzalez et al. (2020), the use of steel wool and steel grit increases indirect tensile strength (ITS) value, stiffness, and resistance to fatigue fracture of asphalt pavement. Besides, the addition of steel fiber does not impair the workability, so it can be compacted with the same compaction energy required for asphalt mixes which do not contain fibers.

Liu et al. (2011) conducted a study with three varieties of steel fibers and found that fibers with a smaller diameter and longer length performed better than those with a larger diameter and shorter length. This is due to improved fiber-to-fiber contact in the former

instance, which results in greater conductivity. In another study by Serin et al. (2012), fiber contents varying from 0 to 2.5% by the weight of optimum binder content were evaluated. It was found that mixes containing 0.75% fiber showed the greatest stability. The research also indicated that high concentrations of very long steel fibers can contribute to the formation of clusters, resulting in lower stability values compared to fiber-free control samples. This observation is consistent with those reported by Tabakovi'c et al. (2019). Tabakovi'c et al. (2019) reported that poor mixing and cluster formation may produce high-temperature zones that impair the specimen's structure.

2.7.4. Synthetic Fibers

Commonly used synthetic fibers in asphalt mixes are polypropylene, polyester, and aramid. The round and smooth microstructure of those fibers help with interlocking with one another, resulting in a higher softening point (Chen et al., 2005).

According to Tanzadeh et al. (2019), the addition of polypropylene fibers to asphalt reduces the binder bleeding by up to 49% and increases strength by up to 50%. Adding glass fibers with polypropylene fibers produces even more promising results. These two combinations of fibers reduce drain down by up to 80% and increase ITS by 65%. Notably, half of this improvement was solely attributable to the presence of polypropylene fibers, which function as a three-dimensional structure in the asphalt mix, thereby enhancing binder stability and strength. On the other hand, the addition of polyester fibers enhanced binders' resistance to raveling and overall stability (Tang et al., 2017).

Ma et al. (2019) investigated the use of modified binder in conjunction with polyester, mineral, and cellulose fibers applied at a rate of 2.5% by weight of aggregate. Polyester-containing mixes performed well in the wet Cantabro test which indicated that

addition of fiber enhanced abrasion resistance and decreased susceptibility to moisture damage. The findings suggested that mixes containing polyester fibers performed well under longer water immersion times and suggested that the fibers substantially enhanced moisture resistance. Moreover, the thermal stress restrained specimen test (TSRST) demonstrated that polyester fibers enhanced resistance to low temperature cracking. However, the use of polyester fibers had a negative effect on the asphalt pavement resilient modulus and strength, as well as its permeability (Ma et al., 2018).

The impact of incorporating polyolefin and aramid fibers into asphalt mixes depends on the binder type. For example, fibers used with unmodified binders are typically more effective than using them with SBS-modified binders (Kassem et al., 2018). Chen et al. (2005) investigated the functioning mechanism of mineral, cellulose, and polyester fibers in asphalt mixes. The findings revealed that mineral fibers with smaller diameters are more durable than polyester fibers with larger diameters due to a greater interfacial area. In terms of tensile strength, however, polyester fibers outperform mineral fibers.

2.7.5. Eco-friendly Materials

To reduce the environmental impact of human activities, the construction industry utilizes eco-friendly materials. These materials can either be made from recycled materials to conserve energy or be designed to minimize natural resource consumption.

Multiple studies have shown that incorporating waste materials such as coconut shells, coconut fibers, chitosan, date seed ash, and waste tire rubber among others into asphalt pavement can enhance the mix's properties **(**Chen and Wong, 2013; Cheng and Wong, 2015; Sangiorgi et al., 2016; Ghabchi et al., 2021). Sangiorgi et al. (2016) investigated the utilization of bentonite, a waste bleaching clay, as a replacement for

limestone fillers in asphalt mixes. The results demonstrated that the substitution of bentonite for limestone did not significantly reduce air void and increased the ITS of the mix. Also, addition of bleaching clay increased the indirect tensile stiffness modulus but particle loss in the mixture was observed to be twice as high as in the reference mixture due to varying embrittlement. According to a study by Zhang et al. (2018), increasing the filler-to-binder ratio reduces particle loss and permeability, regardless of the filler type due to blocking air voids. Chen et al. (2005) conducted a study on the use of fully recycled concrete aggregates (RCAs) in asphalt mixes. The study revealed that RCAs have a high absorptive capacity due to their low density and high porosity which resulted in a high abrasion value. Nevertheless, the abrasion loss, drain down value, and moisture susceptibility were within acceptable ranges. Chen and Wong (2017) reported that hybrid composites (consisting of 78% RCA and 16% glass material) also have a high binder absorption rate, necessitating a higher binder content for adequate bonding.

Mohammadinia et al. (2018) studied the use of recycled ground tires in asphalt pavement. The results demonstrated that the addition of ground tire as aggregate replacement increased the asphalt mix rigidity by strengthening the interfacial bonds. Based on these findings, it was suggested that both recycled concrete aggregates and recycled tire could be utilized in the asphalt pavements without compromising their performance.

CHAPTER THREE: MATERIALS AND METHODS

3.1. Introduction

This chapter presents an overview of the material selection process, test matrices, and tests conducted on EPM and asphalt mixes. The major tasks of this study are: (i) identification of electrospinning parameters; (ii) solution preparation for electrospinning; (iii) production of EPM; (iv) characterization of EPM; (v) preparing laboratory HMA mix; and (vi) performing HWT, SCB and TSR tests on laboratory-prepared mixes and analyze the test results.

3.2. Material Collection and Sample Preparation

3.2.1. Grinding PET Water Bottles

The PET plastic used in this study was obtained from post-consumer PET. To prepare the material for milling, the stickers, caps, and cap rings from bottles were removed and separated the PET plastic. Sorted PET then was cut into pieces no larger than 5 mm x 5 mm and dried at 45°C for 2 hours. According to a study performed by Ghabchi et al. (2021), treating PET plastic pieces at low temperatures increases their fragility, resulting in greater milling effectiveness. For this reason, small pieces of PET were refrigerated at a temperature of -18 °C for a duration of 4 hours prior to grinding them. Next, a commercially available grinder with a double-blade rotor rotating at 15,000 rpm was utilized to grind the approximately 10g of PET particles in each batch. After grinding, the PET particles were passed through a No. 4 sieve with a 4.75 mm mesh size. Any residual particles on the 4.75 mm sieve were added to the following grinding batches after cooling to the targeted temperature. The gradation of ground PET is presented in Figure 3.1.

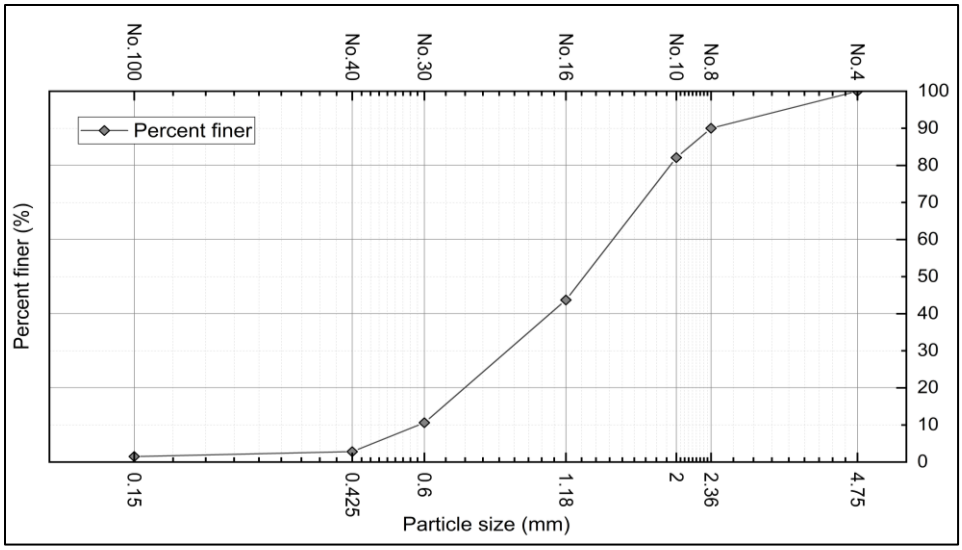

Figure 3.1 Particle size distribution of ground PET

This process was repeated several times until sufficient amount of ground PET was obtained. Figure 3.2 depicts a photographic view of ground PET.

Figure 3.2 Photographic view of ground PET

3.2.2. Collection of Aggregates

Five different stockpiles of aggregates with predetermined gradations (Figure 3.3) were collected from a local asphalt plant. The nominal maximum aggregate sizes (NMAS) for Bin-1, Bin-2, Bin-3, Bin-4, and Bin-5 are as follows: 19.0 mm, 12.5 mm, 4.76 mm, 9.5 mm, and 2.36 mm, respectively. The samples were then transported to the asphalt

laboratory and stored there. The aggregates collected from the stockpiles were then used to produce asphalt mixes.

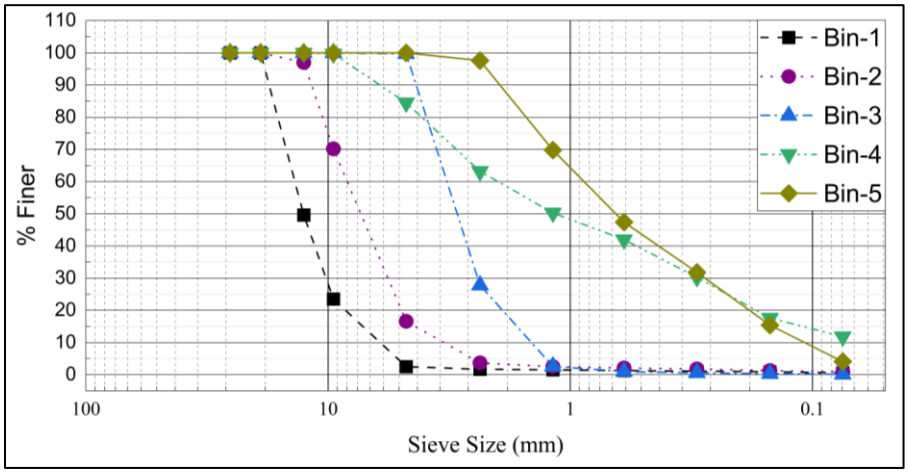

Figure 3.3 Particle size distribution of collected aggregate stockpiles

3.2.3. Collection of Asphalt Binders

Bitumen, also known as asphalt binder, is a highly viscous, black, semi-solid form of petroleum byproduct. It consists of a complex mixture of hydrocarbons and the precise composition of which varies depending on the petroleum source and refining method employed (Selvasofia et al., 2022). A PG 58-28 asphalt binder, widely used in South Dakota's pavement construction projects was collected from a refinery plant in Sioux City, IA.

3.3. Electrospinning Setup

An electrospinning system consists of three main components: a high-voltage power supply (HVPS), a syringe pump with a conductive needle, and a conductive collector (Owida et al., 2022). In this study, an in-house fabricated electrospinning apparatus was used for producing EPM in the lab (Figure 3.4). It is important to note that the two electrodes i.e., nozzle and collector were completely enclosed within a 600 mm x 600 mm

x 450 mm in-house fabricated plexiglass box. Previous studies performed by Ramakrishnan et al. (2019), Cheng et al. (2017), and Schaub et al. (2013) showed that variations in the environment's humidity during electrospinning affect the fiber's diameter and surface texture.

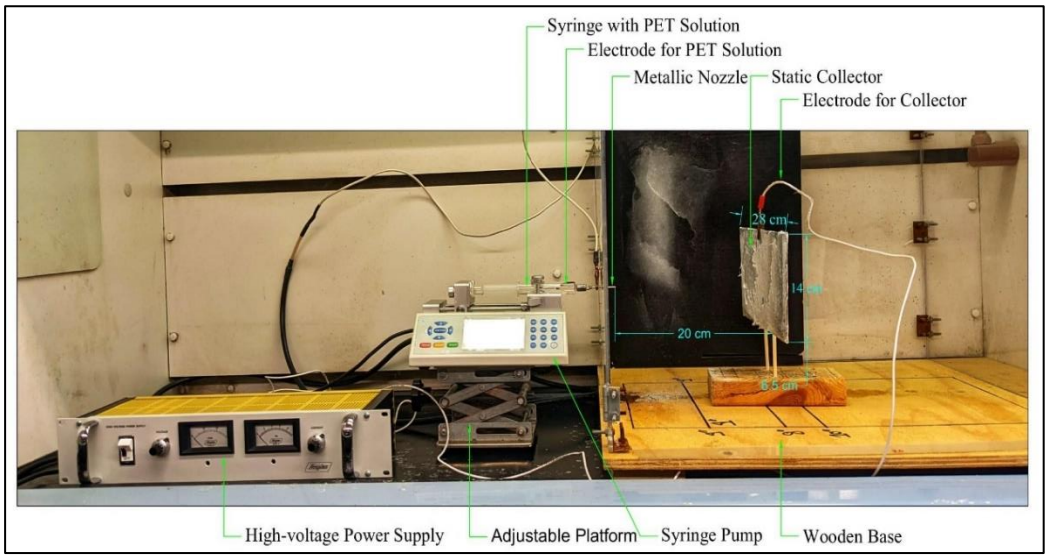

Figure 3.4 A Photographic view of the in-house fabricated electrospinning setup

For this reason, the enclosure of the electrospinning box is important for maintaining the relative humidity of the spinning environment during fiber production to maintain fiber consistency (Schaub et al., 2017). A syringe pump (Fusion 200 two-channel syringe pump) was placed on an adjustable platform outside the plexiglass box. This setup also included a 10 mL glass syringe containing electrospinning solution. A #16 steel needle of 1.26 mm internal diameter was used at the tip of the syringe. The needle was then passed horizontally through a hole (Equivalent to a #10- or 3.0-mm needle diameter) created on the wall of plexiglass box which served as the electrode for the solution. Using aluminum foil, cardboard, wooden sticks and glue, a static collection plate (28 cm x 14 cm) was constructed in the laboratory. This plate was placed inside the plexiglass box and 20 cm

from the tip of the syringe needle. The entire system was then powered by a high-voltage power source.

3.4. Preparing Electrospinning Solution

Dichloromethane (DCM) and trifluoroacetic acid (TFA) from Spectrum Chemical MFG Corp were used as solvents. Solution was prepared using solvent of DCM and TFA in a ratio of 30:70 by volume in a ventilated area. Then, the weight of the solution was measured. Two different polymer solutions comprising 15 and 20% of ground PET by the weight of solvents were prepared (Table 3.1). According to Veleirinho et al. (2008), both TFA and DCM are volatile solvents that can easily evaporate at room temperature and pressure. Therefore, to prevent loss of solvents, the solution container was tightly sealed and kept in a well-ventilated area at the time of mixing. To make the complete dissolution of ground PET possible, solution was stirred using magnetic stirrer at room temperature for 24 hours. The process of preparing PET solution is depicted in Figure 3.5.

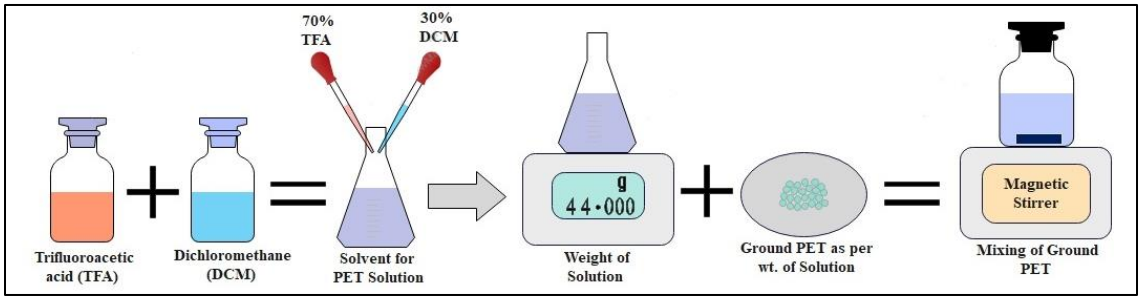

Figure 3.5 Flow diagram of solution preparation from ground PET

3.4.1. Producing PET Fibers

The prepared solution was transferred into a 10 mL glass syringe connected to a #16 needle. Afterward, the syringe was placed in the syringe pump and the discharge rate was set on the pump. The pump and the loaded syringe were placed on an adjustable

platform. The height of the platform was adjusted to allow the needle passing through a hole created in the plexiglass box with its axis opposing the center of the metallic collector. Then the positive and negative electrodes connected to the HVPS were connected to the nozzle (metallic needle) and the conductive collector. HVPS was set to supply 20 kV and the syringe pump was initiated. For each solution type, PET fibers were synthesized at discharge rates of 250, 120, 60, 50, and 40 µL/min (Table 3.1). In order to ensure enough fiber deposition on the plate, the syringe pump was operated for at least 20 minutes for each discharge rate. Afterwards, the EPM mat was collected and set aside for further testing.

Table 3.1 Solution preparation and discharge rate for electrospinning

Solution Types	Ground PET Amount (By wt. of solution)	Discharge Rate (RD) (µL/min)	Electrospinning Parameters
S_1	15%	250 120 60 50 40	Tip-to-Collector Distance: 20 cm Electrospinning Voltage: 20 kV TFA and DCM 70/30 by Volume
S_2	20%	250 120 60 50 40	

3.5. Asphalt Mix Design

3.5.1. Aggregate Structure

Superpave mix design and the available mix designs available for the same materials were consulted to select the aggregate structure. As a result, the collected aggregates from stockpiles, shown in Figure 3.3, were selected to be blended at 15, 20, 15, 30, 20% (total weight of blended aggregate), respectively. The combined gradation of the

aggregate structure has a nominal maximum aggregate size (NMAS) of 12.5 mm as shown in Figure 3.6. Then, FHWA 0.45-power chart was used to evaluate blended aggregate gradation (Figure 3.7).

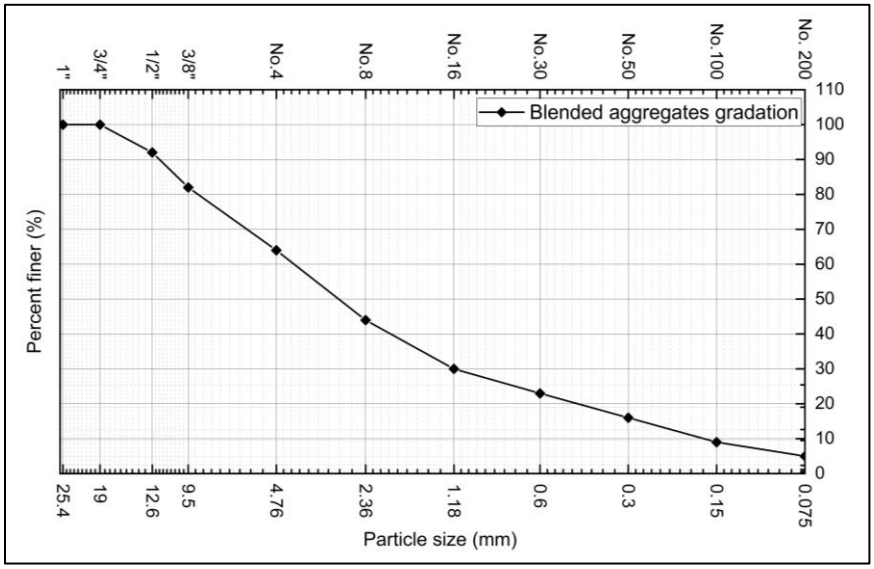

Figure 3.6 Blended aggregates gradation curve

This chart includes the maximum density line that represents particle size distribution required for maximum density which is a straight line based on the Fuller formula (Mamlouk and Zaniewski, 2006). The 0.45th power chart in Figure 3.7 shows that blended aggregates did not align with the maximum theoretical density line and the blended aggregates fell in between upper and lower gradation limits.

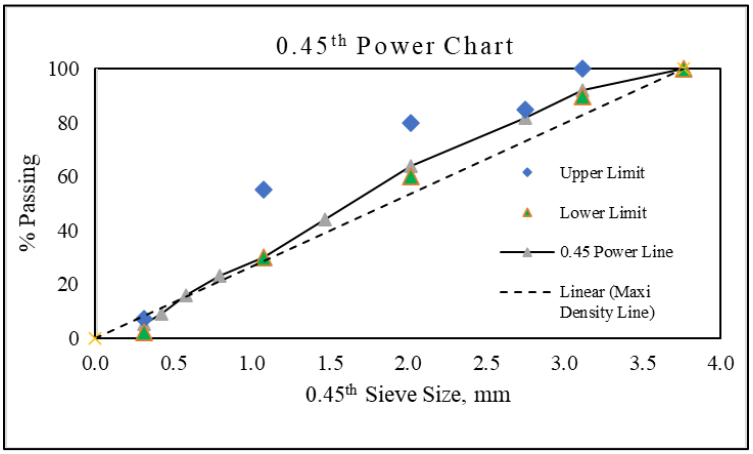

Figure 3.7 The 0.45th chart of blended aggregates

3.5.2. Volumetric Properties of Asphalt Mix

3.5.2.1. Loose Mix Preparation

For each trial of asphalt binder content two identical specimens of loose asphalt mix were prepared to determine the mix maximum theoretical specific gravity (G_{mm}). For this purpose, 1500g of aggregate blend batched according to the determined aggregate structure (section 3.5.1) for each sample was batched (Figure 3.8a). The batched aggregates and PG 58-28 asphalt binder were then heated at 160°C in the oven and mixed (Figure 3.8b). The loose mixes were aged for 2 hours at 135°C in the oven (Figure 3.8c). After 24 hours of cooling the sample in room temperature, the G_{mm} of the trial blend mixes prepared at each binder content was determined according to AASHTO T 209 (AASHTO, 2011) standard method.

Figure 3.8 Determination of G_{mm} value (a) aggregates batching; (b) mixing aggregates and asphalt binder; and (c) de-airing of loose mix

3.5.2.2. Compacting Cylindrical Samples

A Superpave gyratory compactor operated under gyration mode set to compact the

samples at N_{Design} = 75 gyrations according to AASHTO R 35 (AASTHO, 2011).

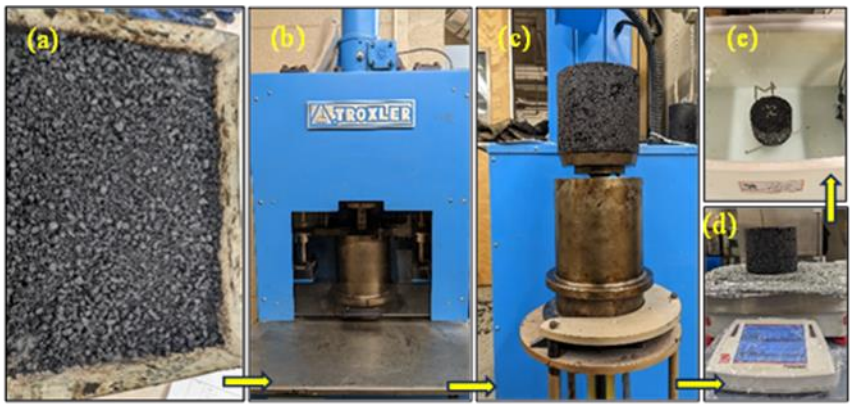

Figure 3.9 (a) loose asphalt mix; (b) SGC compactor; (c) compacted sample; (d) determination of bulk specific gravity of cylindrical samples

To prepare a trial batch of compacted samples the aggregates were batched out to produce a final mix specimen of approximately 4800 g following the specified aggregate batch proportions (section 3.5.1). The heated binder and aggregates were mixed using a bucket mixer. The mix was placed in a flat pan and heated for two hours at 135°C in an oven and stirred in every 30 minutes for short-term aging. For each trial binder content, two specimens were compacted at the design number of gyrations using the Superpave gyratory compactor (Figure 3.9b). The gyratory samples of 150 mm diameter (Figure 3.9c) were compacted according to AASHTO T 312 (AASHTO, 2011). Then, the bulk specific gravity (G_{mb}) of the compacted specimens was determined according to AASHTO T 166 (AASHTO, 2011) standard test procedure (Figures 3.9c and 3.9d).

3.5.3. Optimum Binder Content

To determine the optimum binder content, three different trial binder contents of 4.5, 5.0 and 5.5% were used to prepare asphalt mixes as descry bed in sections 3.5.1 and 3.5.2. For mixes and cylindrical samples prepared with each binder content, G_{mm} and G_{mb} values were determined and important volumetric properties each mix were determined and binder

content corresponding to 4.0% air void was selected as the optimum binder content (5.4%). To check the volumetric properties according to AASHTO M323 (AASHTO, 2011) at optimum binder content, average G_{mm} and G_{mb} at 5.4% binder content were determined from three identical samples (Table 3.2). Table 3.2 Volumetric properties at selected optimum binder content

Table 3.2 Volumetric properties at selected optimum binder content

Properties	Value	AASHTO M323 Requirements	Comment
AV (%), Avg	3.8		
G_{mb} (Avg)	2.353		
G_{mm} (Avg)	2.446		
Density, (Avg) %	96.2		
VMA, (Avg) %	15.1	>14	OK
VFA, (Avg) %	74.7	65-78	OK
P_{be}, %	4.8		
DP	0.9	0.6-1.2	OK
G_{mb} @ N_{ini} (Avg)	2.175		
Density @ N_{ini} (Avg)	88.9	<90.5	OK

3.6. Preparation of Asphalt Mixes for Performance Tests

Asphalt mixes were prepared by batching aggregates and PG 58-28 asphalt binder in accordance with the asphalt mix design and then adding 0, 0.5, 1.0 and 1.5% of EPM to produce HMA-C, HMA + 0.5% EPM, HMA + 1.0% EPM and HMA + 1.5% EPM mixes, respectively (Table 3.3).

Table 3.3 Different HMA mix preparation and their test matrix

Asphalt Binder Types	EPM (%)	Mix Type	Asphalt Mix Characterization		
			SCB	HWT	TSR
PG 58-28	0.0	HMA-C	✓	✓	✓
	0.5	HMA + 0.5% EPM	✓	✓	✓
	1.0	HMA + 1.0% EPM	✓	✓	✓
	1.5	HMA + 1.5% EPM	✓	✓	✓

The size of the fiber used in mix preparation was 3 mm x 35 mm (Figure 3.10). The addition of EPM to the mix followed a 15-second dispersion method that was previously utilized by Alfalah et al. (2020).

Figure 3.10 EPM used for the preparation asphalt mix

For this purpose, the EPM was first split into three equal weight portions. Then, the preheated aggregates were added along with the binder into the bucket mixer bowl (Figure 3.11a) and mixed to consistency. Then, the first portion of the EPM was gradually added while mixing progressed until a consistent mix was produced and no fibers were visible. This process was repeated until all EPMs were added into the mix. Mixing was then continued until no fibers were visible. After that loose asphalt mixes (Figure 3.11c) were kept for further laboratory aging and HMA sample preparation (Figure 3.11d).

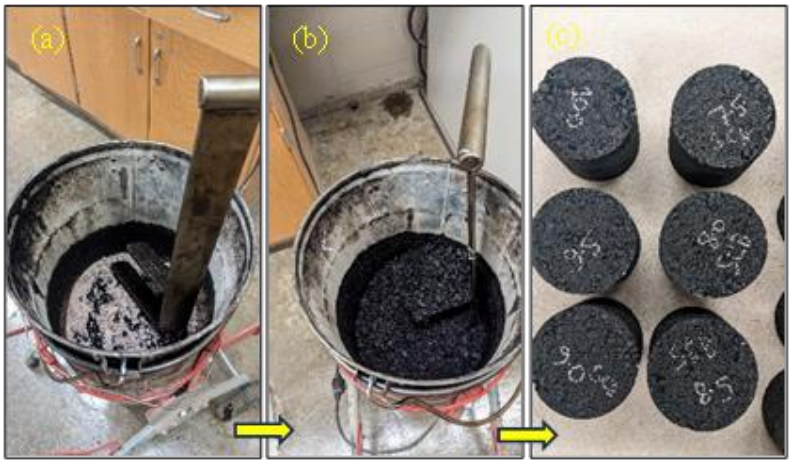

Figure 3.11 (a) Mixing asphalt in a bucket mixer; (b) addition of EPM to mix; and (c) final mix containing EPM

3.7. Fiber Characterization

3.7.1. Tensile Strength of Produced EPM

In the electrospinning process, the presence of lateral instability and different travel distances from the nozzle to the collection plate cause nonuniform fiber deposition. Consequently, the fiber thickness, parallel to the axis of nozzle, is higher at the center of the collector and gradually decreases toward the edges. In addition, it is not feasible to test individual fibers because the resulting single fiber is small, and the produced fiber mat has a nonwoven structure (Ghabchi and Castro, 2021). For this reason, to determine the tensile strength of EPM, the method proposed by Ghabchi and Castro (2021) was applied. In this method, constant weight and approximately the same cross-sectional area were maintained in every sample. Therefore, to prepare the identical specimens for tensile strength test, the EPM mat deposited in the center of the plate was carefully collected from the static collector and allowed to dry for a minimum of 24 hours in a ventilated chamber at room temperature and to eliminate any residual solvent. Later, the loose mat was placed on aluminum foil (Figure 3.12a) and folded in multiple directions as depicted in Figure 3.12b. The EPM mat along with the aluminum foil, was then cut into an approximate size of 115 mm x 140 mm. Next, the weight of the resized EPM mat was determined on a scale to 0.001g of accuracy (Figure 3.12c). If the weight of the strip exceeded the designated amount, it was readjusted by removing a very thin layer from the strip utilizing a sharp utility knife (Figure 3.12e**)**. After achieving the specified weight (Figure 3.12f) and dimensions, pieces of sandpaper on both ends of the fiber strip were glued (Figure 3.12g). The glue strip was then kept aside for at least 2 hours before testing to allow the glue to dry completely. Based on observations, the glued sandpaper served two purposes. Firstly,

it kept the two or more layers of EPM strips together and assisted them to perform like a single-layered mat. Secondly, it provided additional grip to the jaws of loading frame. During the transfer of the EPM strip to the loading frame, care was taken to ensure that the outer edge of jaws grasped the EPM mat and applied tensile force to the mat (Figure 3.12h). Finally, tensile strength test was conducted using a loading frame provided by Texture Technologies Corp., USA (Figure 3.12i).

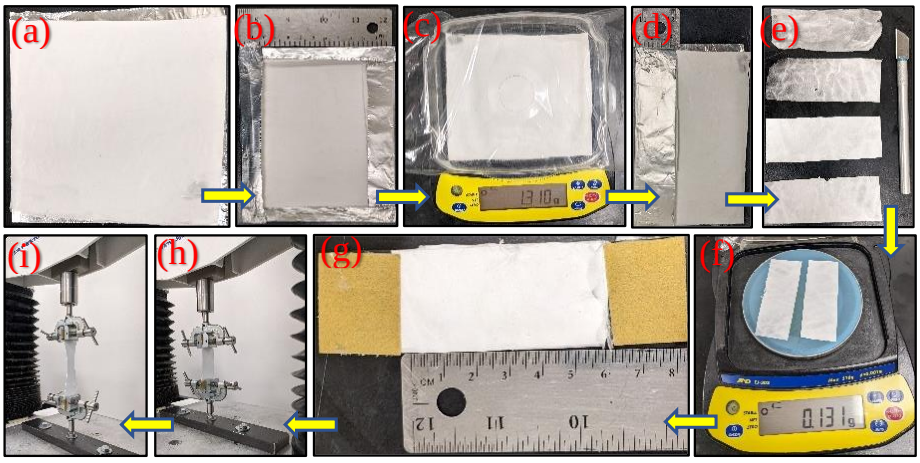

Figure 3.12 EPM's tensile strength test (a) EPM on aluminum foil; (b) folding along its edge; (c) weighting the 115 mm x 140 mm fiber mat; (d) folding the EPM mat along its long edge for strip preparation; (e) adjusting the EPM 50 mm x 27 mm fiber's strip to 0.130 g weight; (f) checking the EPM strip weight; (g) gluing the both end of the strip using sandpaper; (h) clamping the EPM strip on the loading frame; and (i) testing the EPM strip using loading frame of Texture Technologies Corp., USA .

The sample was subjected to tensile force at a rate of 2 millimeters per minute. Four identical specimens were tested for each discharge rate, and the specimens' tensile strength was determined by analyzing the load and displacement data collected.

3.7.2. Scanning Electron Microscopy (SEM) Tests

The morphology of the produced EPM was determined using a SEM device (S-3000N, Hitachi Co., Tokyo, Japan). To achieve this goal, the EPM fibers (Figure 3.13a)

were first coated with a layer of gold-palladium using a CrC-150 sputtering machine (Figure 3.13b). Then, a conductive adhesive was used to attach the EPM to the SEM sample base and before that EPM from Plasma Science Inc., USA (Figure 3.13c).

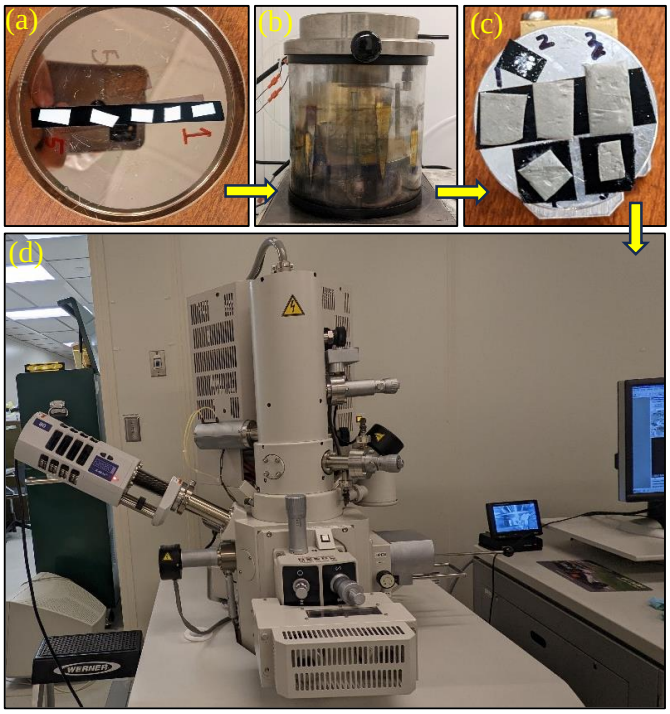

Figure 3.13 SEM micrograph collection procedures (a) gluing the EPM for coating; (b) coating the EPM mat; (c) coated EPM placing in SEM sample base and (d) SEM imaging

The thickness of the coating layer was 0.15 kA. The SEM test was carried out using a 20 kV accelerating voltage (Figure 3.13d) to ensure good resolution of SEM micrograph. From SEM micrograph, the diameter of the EPM was measured using the image processing software ImageJ, which was developed by the National Institutes of Health of the United States.

3.7.3. Fourier-Transform Infrared (FTIR) Spectroscopy

FTIR spectroscopy was employed to investigate the chemical compositions of EPM and the presence of residual solution in the EPM mat after production. Additionally, this

test provided information about any chemical changes in the EPM compared to PET. FTIR spectroscopy was performed using a PerkinElmer Universal ATR (Perkin–Elmer Corporation, Norwalk, Connecticut, USA). The samples were placed in contact with the ATR element (ZnSe crystal, 45° ends) at room temperature. For this purpose, desiccated samples were tested at a wavenumber range of between 4000 and 350 cm^{-1}.

3.8. Asphalt Mix Characterization

3.8.1. Hamburg Wheel Tracking (HWT) Test

To assess the susceptibility of asphalt mixes to rutting and potential for moisture-induced damage, the HWT test in accordance with AASHTO T 318 (AASHTO, 2011) standard method was conducted. Samples were compacted in a SGC to a diameter and height of 150 mm and 60 mm, respectively. According to the AASHTO T 269 (AASHTO, 2011) standard, the bulk specific gravity values (G_{mb}) of the resulting cylindrical samples were determined. For the HWT tests, compacted asphalt samples 7.0 ± 0.5% air voids were used.

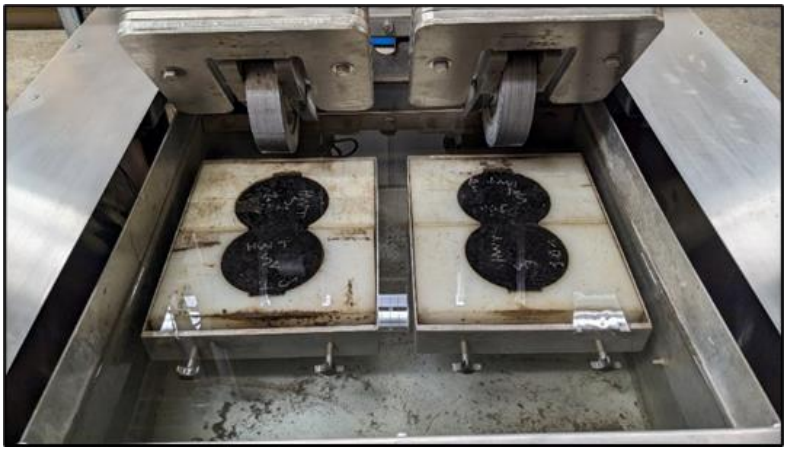

Figure 3.14 HWT device with HMA sample

Two pairs of cylindrical samples were cut to the desired shape and placed in plastic molds, in the HWT machine for testing (Figure 3.14). The testing procedure involved

moving a steel wheel with a load of 705 N back and forth over the surface of the HMA specimens that were submerged in a constant-temperature water bath set to 50 ± 1 °C, as specified by the standard. The machine's steel wheels have a diameter of 203 mm and a width of 47 mm and oscillate at a rate of 52 ± 2 passes per minute. After each pass, the machine uses a linear variable differential transformer (LVDT) to determine the relative vertical deformation of the sample (Zhang et al., 2021; Lv et al., 2020). The test was programmed to end autonomously after either 20,000 passes or 12.5 mm of maximum vertical deformation, whichever occurs first.

3.8.2. Semi Circular Bend (SCB) Test

The SCB fracture test is widely utilized to evaluate the fracture energy and cracking resistance of the asphalt mixes (Limón-Covarrubias et al., 2019). The SCB tests (Figure 3.15) were conducted in accordance with the method outlined in D8044 (ASTM, 2017) standard. Using a Superpave gyratory compactor, samples with a diameter of 150 mm and a height of 135 mm were compacted to obtain final SCB samples with air void of 7.0 ± 0.5%. Subsequently, specimens with a thickness of 57 ±1 mm were cut from the compacted samples by discarding the top and bottom sections of the 135 mm tall specimen, which measured 15 ± 5 mm in length. After preparing the circular specimens as previously described, they were cut along their cross-sections' diameter to obtain two semicircular half-cylinders. Air void of each semicircular half-cylinder sample was determined, followed by aging them at 85°C for a duration of 120 hours. Then using a precision saw, notch depth of 25, 32, and 38 mm were precisely cut as specified by ASTM D8044 (ASTM, 2017). Then, four SCB specimens were evaluated for every notch of depth. Before performing the SCB test, all specimens were conditioned for two hours at 19°C

corresponding to the intermediate temperature range at which most of the traffic load is applied. Throughout the SCB test, the semicircular specimens were loaded monotonically until fracture. The test was conducted by loading the specimen in its midspan at a constant rate of 0.5 mm/min in a three-point bending load configuration.

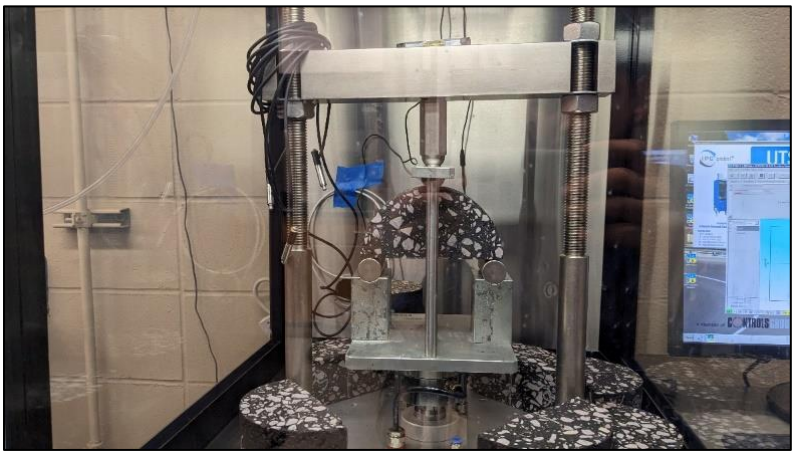

Figure 3.15 SCB testing machine with environmental chamber

To determine the J-integral (J_c) the Equation 3.1 was used.

$$Jc = -\left(\frac{1}{b}\right)\frac{dU}{da} \tag{3.1}$$

where:

J_c = critical strain energy release rate (kJ/m^2),
b = sample thickness (m),
a = notch depth (m),
U = strain energy to failure (kJ), and
dU/da = change of strain energy with notch depth (kJ/m).

3.8.3. Tensile Strength Ratio Test

AASHTO T283 (AASHTO, 2011) standard procedure was followed to evaluate the moisture sensitivity of asphalt mixes. A SGC was used to prepare specimens with a diameter of 150 mm and a height of 95 ± 5 mm, with air voids of 7.0 ± 0.5%. Three specimens from each HMA type were kept under dry conditions (dry specimens), while

the remaining three specimens were conditioned (wet specimens). The conditioning of specimens consisted vacuum saturating them for five minutes by applying 28 kPa absolute pressure. After that, saturated surface dry sample was prepared, and mass of the specimens was measured to determine the percentage of saturation. If the percentage of saturation was less than 70%, the specimens were subjected to more vacuum saturation. If the saturation level was above 80%, the specimen was considered damaged and discarded. To attain a saturation level between 70 and 80%, lower vacuum times and pressures were used. Following saturation, the specimens were wrapped in cling wrap and placed in plastic airtight bags along with 10 mL of water and kept at -18 °C for 16 hours. Next, they were transferred to a water bath of 60 °C and kept for 24 hr. The specimens were then kept in water at 25°C for two hours before testing them in an IDT jig. The conditioning and testing steps are depicted in Figure 3.16.

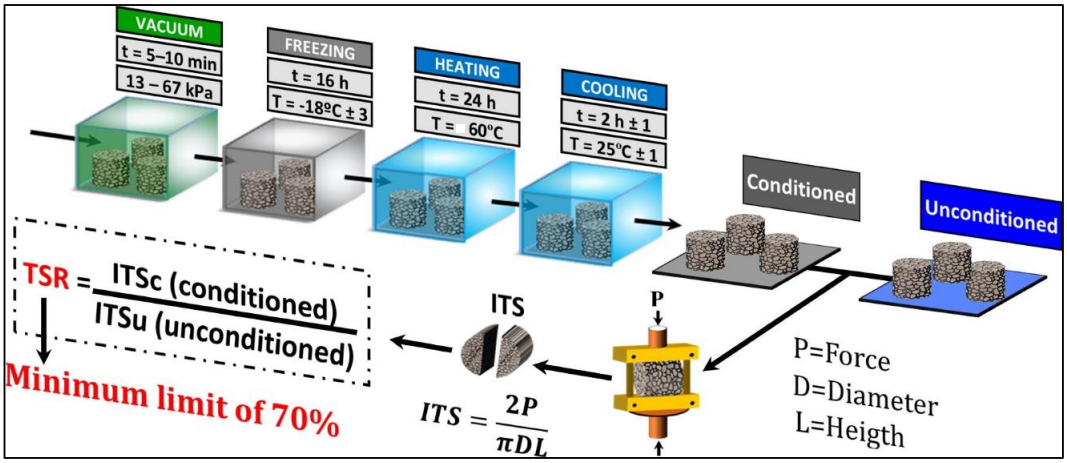

Figure 3.16 Sample conditioning steps for TSR test (after Junior et al., 2019)

The ITS test involves loading the specimen at a rate of 5.08 cm (2 inches) per minute until failure (Figure 3.17). The indirect tensile strength of all six specimens were then calculated using the given Equation 3.2.

$$\mathrm{ITS} = \frac{2\mathrm{F}}{\pi \mathrm{tD}} \tag{3.2}$$

where, ITS is the indirect tensile strength (kPa), F is the force at failure (kN), t is the thickness of the asphalt specimen (m) and *D* is the asphalt diameter (m).

Figure 3.17 (a) TSR test setup; and (b) failure surface

The average indirect tensile strength of the three dry and wet specimens were calculated separately. Equation 3.3 was used to determine the moisture sensitivity or stripping potential of the asphalt.

$$\text{TSR} = \frac{\text{ITS wet}}{\text{ITSdry}} \text{ x } 100 \qquad (3.3)$$

where, TSR is the indirect tensile strength ratio (%), ITS_{wet} is the average indirect tensile strength of the wet specimens (kPa) and ITS_{dry} is the average indirect tensile strength of the dry specimens (kPa).

CHAPTER FOUR: TEST RESULTS OF PET FIBERS

4.1. Introduction

This chapter presents results and discussions pertinent to the results of the tests conducted on EPM produced in the laboratory by changing the electrospinning parameters, namely discharge rates and PET concentration in the solution.

4.2. Chemical Characterizations of PET Fibers

FTIR spectroscopy is a chemometrics method used to analyze chemical compounds and functional groups through studying molecular vibrations (Schmitt and Flemming, 1998). FTIR spectrum is interpreted through comparing it to reference spectra to identify the functional groups present in the sample in the diagnostic region (4000-1500cm^{-1}) of the IR spectrum. In addition, the fingerprint region (1500-400cm^{-1}) of the same spectral graph is used to determine various deformations of molecular structure (P. Gable, 2022).

Figure 4.1 depicts the IR spectra of the EPM obtained at various PET concentrations and discharge rates, as well as the ground MPET. These spectra illustrated the sample's absorbance of infrared radiation as a function of wavenumber. In FTIR spectra, the plot of absorbance versus wavenumber showed peaks that relate to specific vibrational modes of molecules present in the sample. Four distinct and major spectral peaks were observed in Figures 4.1a and 4.1b, which complied to the inherent structure of PET as well as EPM. One of these peaks was located in the diagnostic region at 1715cm^{-1}, while the remaining three were located in the fingerprint region at 1245, 1095, and 715cm^{-1}, respectively. Using the known IR spectrum table by frequency range from Chemistry LibreTexts (Infrared Spectroscopy Absorption Table, 2020), it was determined that the

peaks match the following functional groups: ester carbonyl (C=O) at 1715cm^{-1}, C–O asymmetric and symmetric stretching at 1245 and 1095cm^{-1}, respectively, and C–H wagging vibrations from aromatic structures at 725cm^{-1}. In addition, minor peaks at 1410, 1015, and 875cm^{-1} were observed in each sample. However, it was observed that none of these minor peaks demonstrated a significant difference between the spectra of PET samples cut from the waste PET and the EPM mat prodded in the lab.

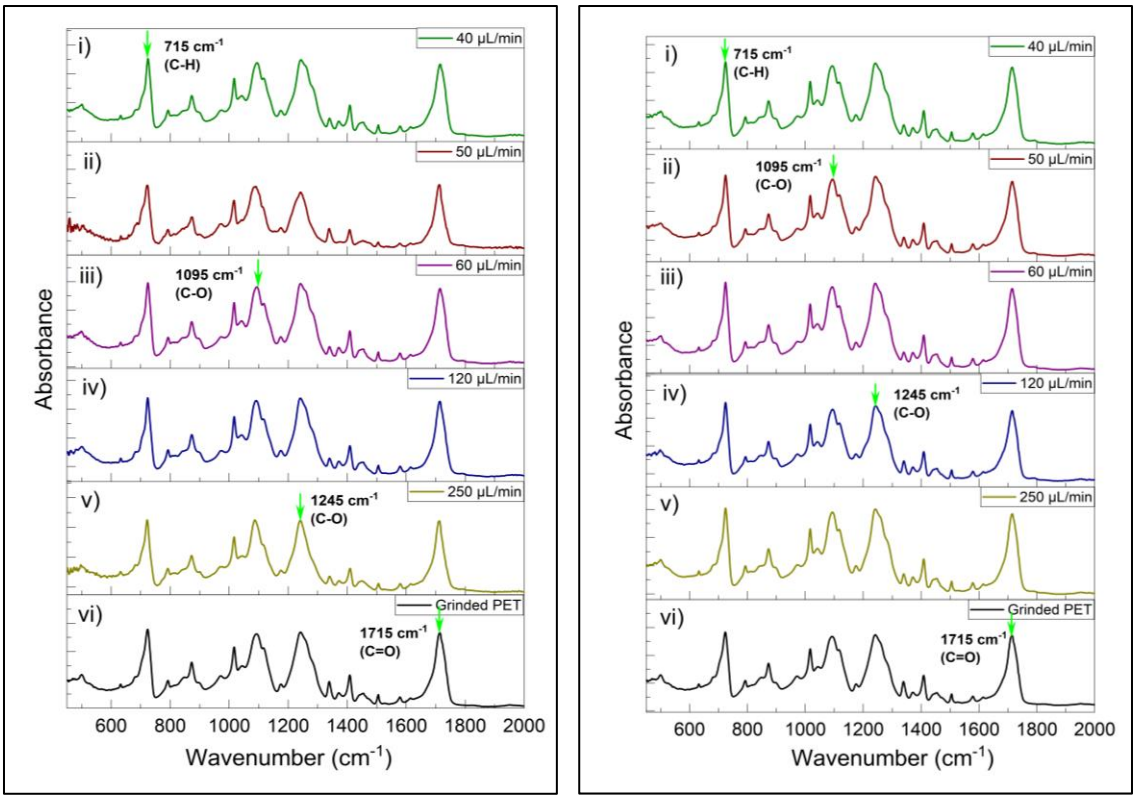

a) 15% PET concentration b) 20% PET concentration

Figure 4.1 IR-Spectra of ground PET and produced EPM at different concentrations of MPET (a) 15% PET concentration and (b) 20% PET concentration

The IR spectra of all EPM samples, including those produced from different concentrations of PET, exhibited identical spectra to that of the ground PET sample. Therefore, it can be concluded that the electrospinning process and the use of TFA and DCM reagents in the preparation of different PET solutions did not cause any chemical

alterations to the PET's chemical structure. Also, drying process applied for the produced fiber was found to be efficient that did not leave any traces of solvent in the produced fibers. For example, if trifluoracetic acid was present in the fiber mat after air-drying the samples for 24 hours, it should have been visible within the 1400-1000cm^{-1} region of IR spectra, due to the presence of trifluoromethyl (-CF_3) functional group. Similarly, the dichloromethane (C-Cl) symmetric and asymmetric stretching should have appeared in the 850-550cm^{-1} range if any trace of this reagent was present in the fiber. As no distinguished peaks correlating with the trifluoromethyl (-CF_3) group or the dichloromethane (C-Cl) symmetric and asymmetric stretching were observed in the IR spectra of desiccated fiber mat compared to that of ground PET, it can be concluded that the natural drying process allowed for the complete evaporation of all solvents used in the production of the EPM mat.

4.3. Effect of PET Concentration and Solution Discharge Rate on Fiber Diameter and Size Distribution

Figures 4.2 and 4.3 show the SEM micrographs of produced EPM using two different PET concentrations, namely 15 and 20% by solution weight. For production of EPM using each PET concentration, five different discharge rates, namely 40, 50, 60, 120, and 250 μL/min were applied. From the SEM micrographs, the size distribution of fibers was determined by analyzing them in ImageJ software with the help of DiameterJ plugin. To determine the average diameter of the fibers produced at each discharge rate, a histogram obtained from ImageJ data was generated in OriginLab software.

It can be observed that the average fiber diameter increased with increasing discharge rate for both types of fibers produced by PET concentrations of 15 and 20%.

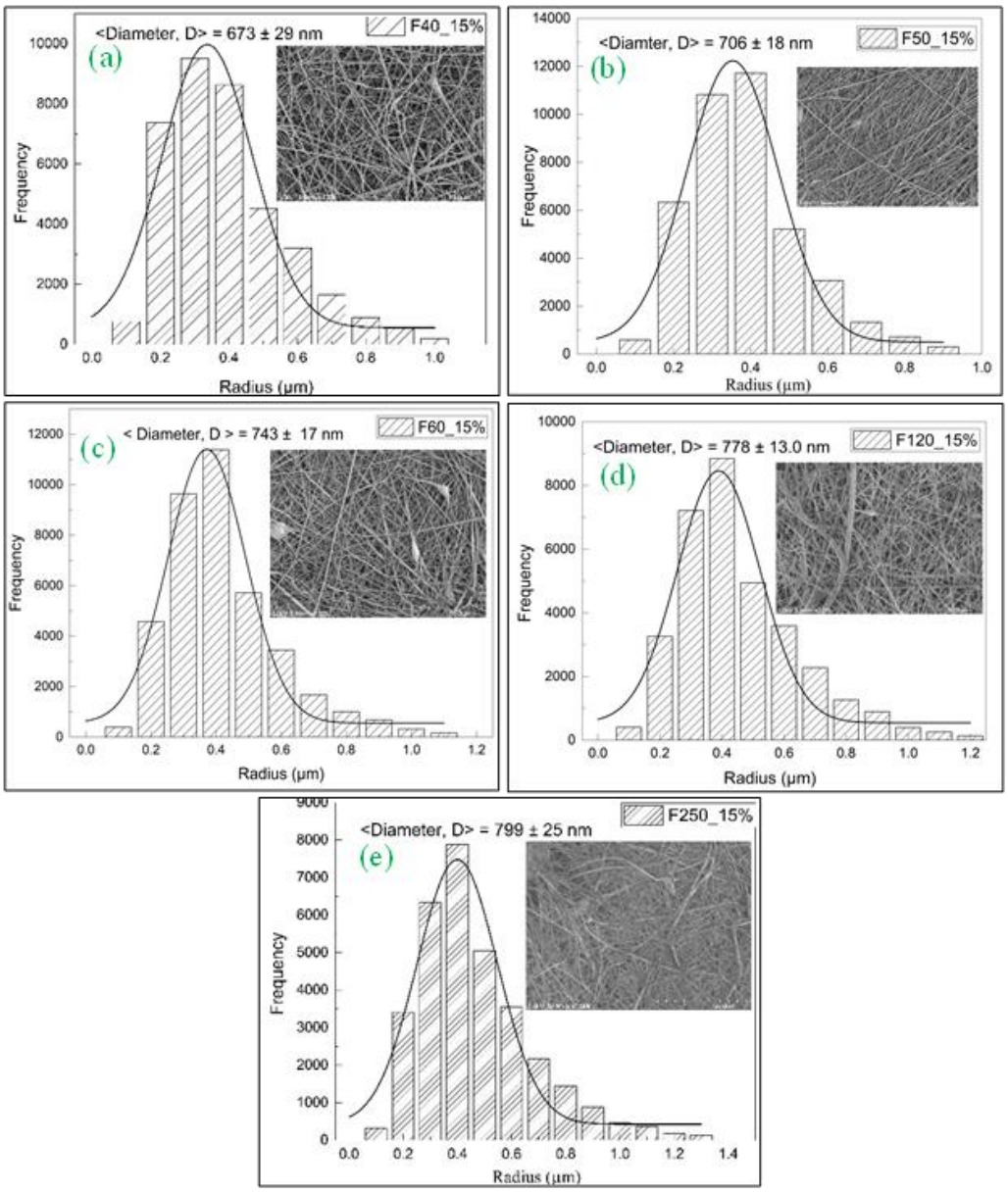

Figure 4.2 SEM micrographs of EPM formed at 15% PET concentration and different discharge rates (a) 40 μL/min; (b) 50 μL/min; (c) 60 μL/min; (d) 120 μL/min and (e) 250 μL/min

Particularly, when 15% PET concentration was used in the solution, the mean fiber diameter increased from 673 nm (Figure 4.2a) for 40 μL/min discharge rate to 706, 743, 778, and 799 nm (Figures 4.2b, c, d and e) when discharge rates of 50, 60, 120, and 250 μL/min were applied, respectively. Similarly, when a concentration of 20% PET was used in the solution, the average fiber diameter increased from 735 nm at 40 μL/min (Figure

4.3a) discharge rate to at, with intermediate values of 746, 770, 778, and 792 nm (Figure 4.3b, c, d and e) at 50, 60, 120, and 250 μL/min discharge rate, respectively.

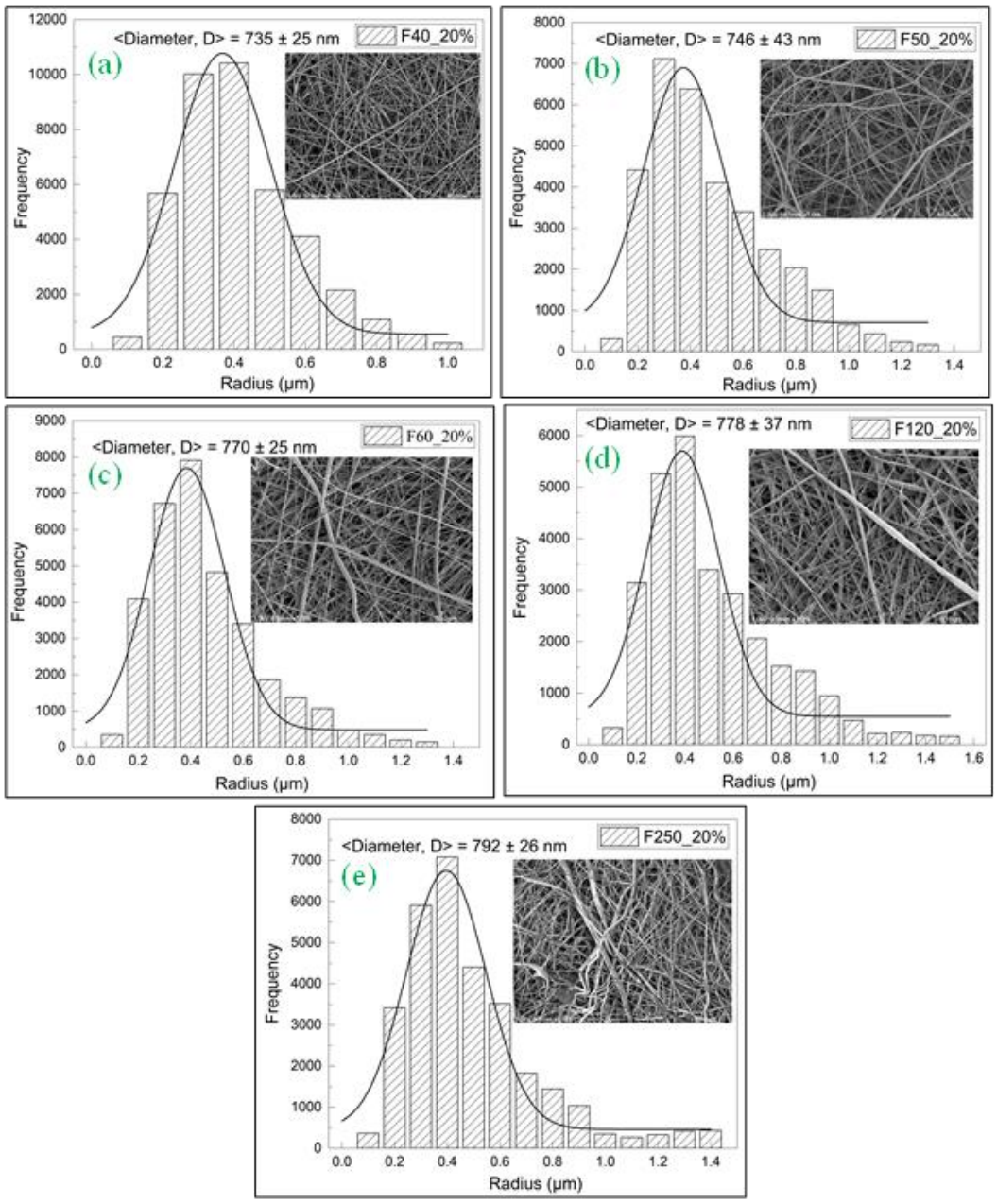

Figure 4.3 SEM micrographs of EPM formed at 20% PET concentration and different discharge rates (a) 40 μL/min; (b) 50 μL/min; (c) 60 μL/min; (d) 120 μL/min and (e) 250 μL/min

It can be concluded that, when MPET concentration was kept at 15%, the effect of the solution discharge rate on the average fiber diameter was significantly higher than those

observed in EPMs produced at 20% PET concentration. This behavior was due to change in the solution's viscosity as a result of increasing PET concentration which affected the electrospinning jet (Bonfim et al., 2021).

The polymer concentration plays a major role in determining the viscosity of the solution, which in turn influences the speed of flow and fiber elongation during electrospinning. The elongation of the jet impacts the diameter of the resulting fibers, with thinner fibers forming from elongated jets and thicker fibers forming from jets with less elongation (Bonfim et al., 2021). Therefore, the higher concentration of PET (20%) in TFA and DCM solution increased the viscosity of the solution compared to the experiments conducted using 15% PET concentration. An increase in solution's viscosity made it more difficult for the electrospinning jet to elongate, leading to larger fiber diameters, as observed in the samples with a 20% PET concentration.

In addition, consistent with the findings of Strain et al. (2015), changing the discharge rate by a factor of six (at a given concentration) had a marginal effect on the thickness of the fibers at higher concentrations. This suggests that the effect of the discharge rate on the fiber diameter was less significant at higher PET concentrations, possibly because of the viscosity of the solution. In contrast, solutions with low concentrations and discharge rates demonstrated less resistance to the deformation of the fiber caused by the applied electric field which resulted in thinner fiber formation (Cho et al., 2020; Lasprilla-Botero et al., 2018**)**.

4.4. Effect of PET Concentration and Solution Discharge Rate on Fiber Morphology

Multiple studies have demonstrated that the characteristics of electrospun fibers are

mostly determined by polymer type, solution properties (such as concentration), and various parameters such as applied voltage and discharge rates (Chen et al., 2008). Figures 4.4 and 4.5 depict SEM micrographs of EPM produced from two concentrations of PET, namely 15 and 20%, in a 70/30 TFA/DCM solution.

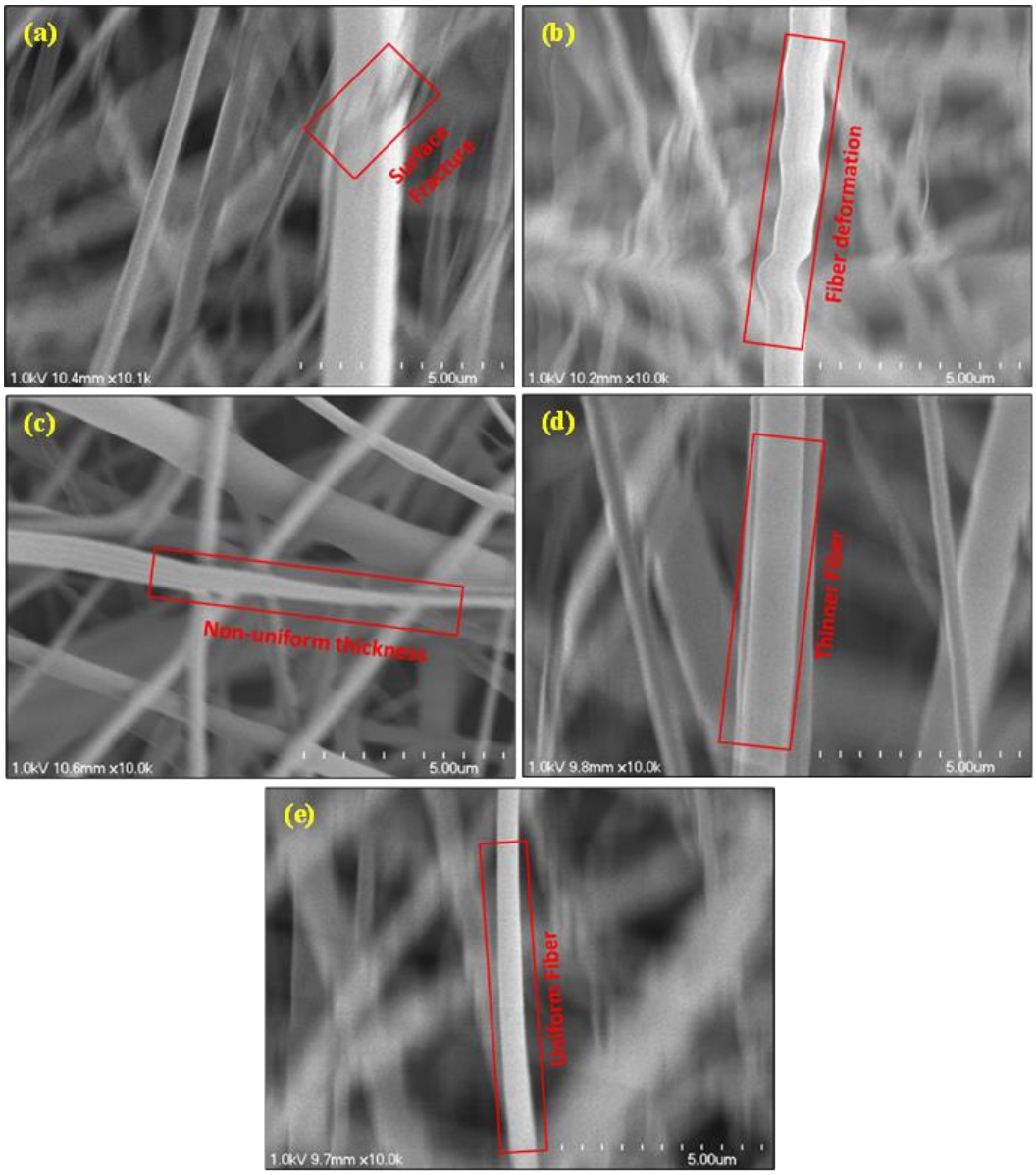

Figure 4.4 SEM images of 15% PET concentration and different discharge rates (a) 250 µL/min; (b) 120 µL/min; (c) 60 µL/min; (d) 50 µL/min and (e) 40 µL/min showing the morphology of EPM

As shown in the SEM micrographs, reducing the discharge rate during electrospinning

eliminated beaded structures and resulted in the formation of thinner, more cylindrical fibers.

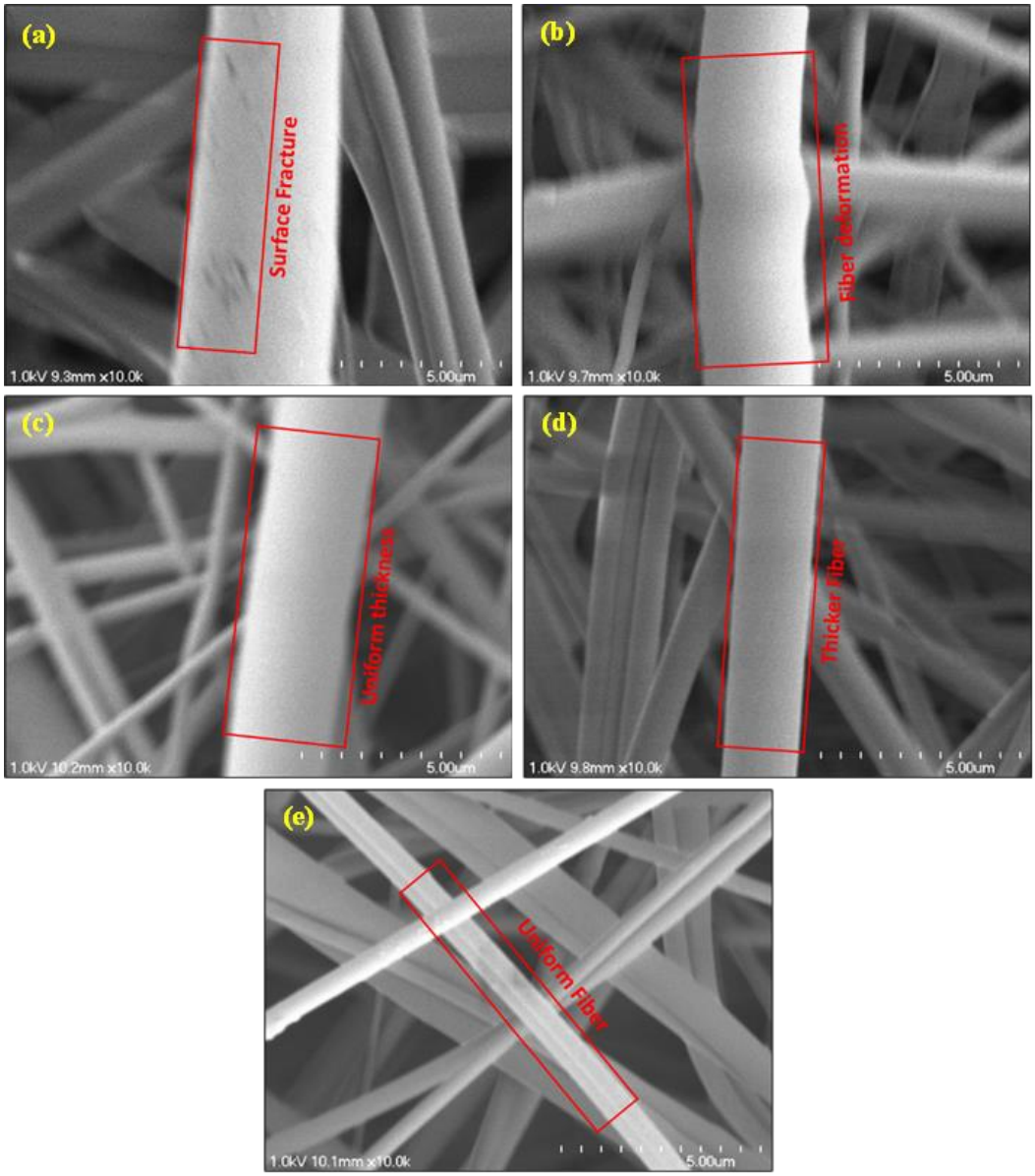

Figure 4.5 SEM images of 20% PET concentration and different discharge rates (a) 250 µL/min; (b) 120 µL/min; (c) 60 µL/min; (d) 50 µL/min and (e) 40 µL/min showing the morphology of EPM

When the discharge rate is excessively high, the solution jet may not be completely stretched by the electrostatic field, resulting in larger droplets and ultimately the production of thicker and defective fibers. Conversely, decreasing the discharge rate can result in the

production of fibers with a reduced diameter and smoother surface (Mercante et al., 2017). To achieve smooth and continuous fibers, different electrospinning parameters were changed and their effect on the EPM's quality was investigated. Specifically, PET concentrations of 15 and 20%, as well as discharge rates ranging from 250 to 40 μL/min were examined in this study. The discharge rate of the solution through the needle has a significant effect on the size of the droplets (Zong et al., 2002).

Conversely, increasing the concentration of MPET in the solution produced fibers with more uniform morphology. Upon analysis of the SEM images of Figure 4.4 and 4.5 obtained at a discharge rate of 250 μL/min, it was observed that both concentrations of PET resulted in fibers with surface fractures. In contrast, when the discharge rate was decreased to 120 μL/min, the produced fibers did not exhibit fractures on their surfaces, rather they displayed deformations in their morphologies, as shown in Figures 4.4b and 4.5b for both concentrations. When the discharge rate was further decreased to 60 μL/min, the resulting fibers showed a non-uniform thickness at a concentration of 15% PET (Figure 4.4c), whereas fibers with a uniform morphology were observed at a concentration of 20% PET (Figure 4.5c). The discharge rates of 50 (Figures 4.4d and 4.5d) and 40 μL/min for both concentrations resulted in even more uniform fibers in comparison with their subsequent higher discharge rates as shown in Figure 4.4e and 4.5e although the thickness of the fibers generated at various concentrations and discharge rates varied. This phenomenon is predominantly attributable to the opposition between the surface tension effect and the increase in solution viscosity and discharge rate, which causes the solution-air interface to expand (Aydemir and Demiryürek, 2022). As the discharge rate increased, so does the quantity of solution flowing through the needle, resulting in a jet that was unstable and

produced to larger diameter distributions. In addition, it has been observed that there exists an optimal viscosity and discharge rate that produces a stable and continuous flow, allowing for the defect-free production of fibers (Haider et al., 2018). In this case, beyond discharge rate of 120 μL/min, uniform and defect-free fibers began to form for both concentrations of PET.

In summary, the fibers with the highest degree of uniformity were consistently generated at the lowest spinnable discharge rate, regardless of the viscosity and discharge rate, because fibers produced at lower discharge rates exhibited a smooth and cylindrical shape, and their surface was free of structural defects.

4.5. Mechanical Properties of EPM Fibers

The mechanical characteristics of EPM were evaluated by conducting uniaxial tensile tests. Figure 4.6 displays a typical force-strain curve derived from the tensile test conducted on the EPM mat. During the initial phases of the test, an entanglement behavior was observed. This behavior manifested itself as elongation in the EPM mat without a significant increase in measured load (soft behavior). From SEM tests, it was found that the filaments within the EPM mat were entangled and randomly aligned. When it was subjected to the load, the fibers, before undergoing stretching, needed to un-entangle and align in the load direction. Therefore, initial strain without significant loads at the beginning of the test was observed (Figure 4.6). Subsequently, the EPM mat exhibited elastoplastic behavior characterized by significant deformations.

The results indicated that, right after the un-entanglement zone, the fibers showed linear elastic behavior until they reached the yield point, at which the slope of the force

strain curve declined. At higher strains, however, the fibers showed large deformations and presented plastic behavior.

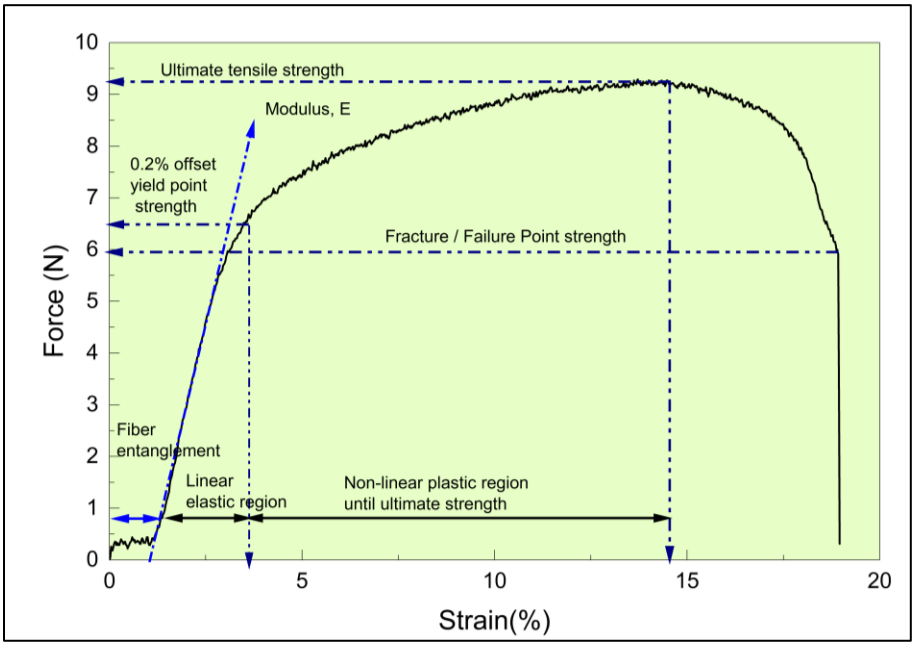

Figure 4.6 A typical force-strain curve of EPM mat

The linear elastic region of the stress-strain graph of EPM was defined by two key parameters: Modulus (E) and the force corresponding to yield ($F_{0.2\%\ offset}$) determined by 0.2% offset of strain parallel to the slope of the linear section. On the other hand, the non-linear plastic region was characterized by three parameters: force corresponding to ultimate strength (F_{ult}), ultimate strain (ε_{ult}), and toughness (T), which corresponds to the area beneath the force-strain curve up to ultimate force. The relationship between mechanical properties and fiber diameters (from SEM images) is depicted in Figure 4.7. Figures 4.7a and 4.7b show that the force corresponding to the ultimate strength and strain of EPM decreased as fiber diameters increased. In other words, an increase in EPM's diameter resulted in a reduction in the strength and ductility of the produced fibers. Specifically, the force corresponding to the ultimate strength was found to decline from 6.54 N to 1.14 N for a PET concentration of 15% as the fiber diameter increased from 673 nm to 799 nm.

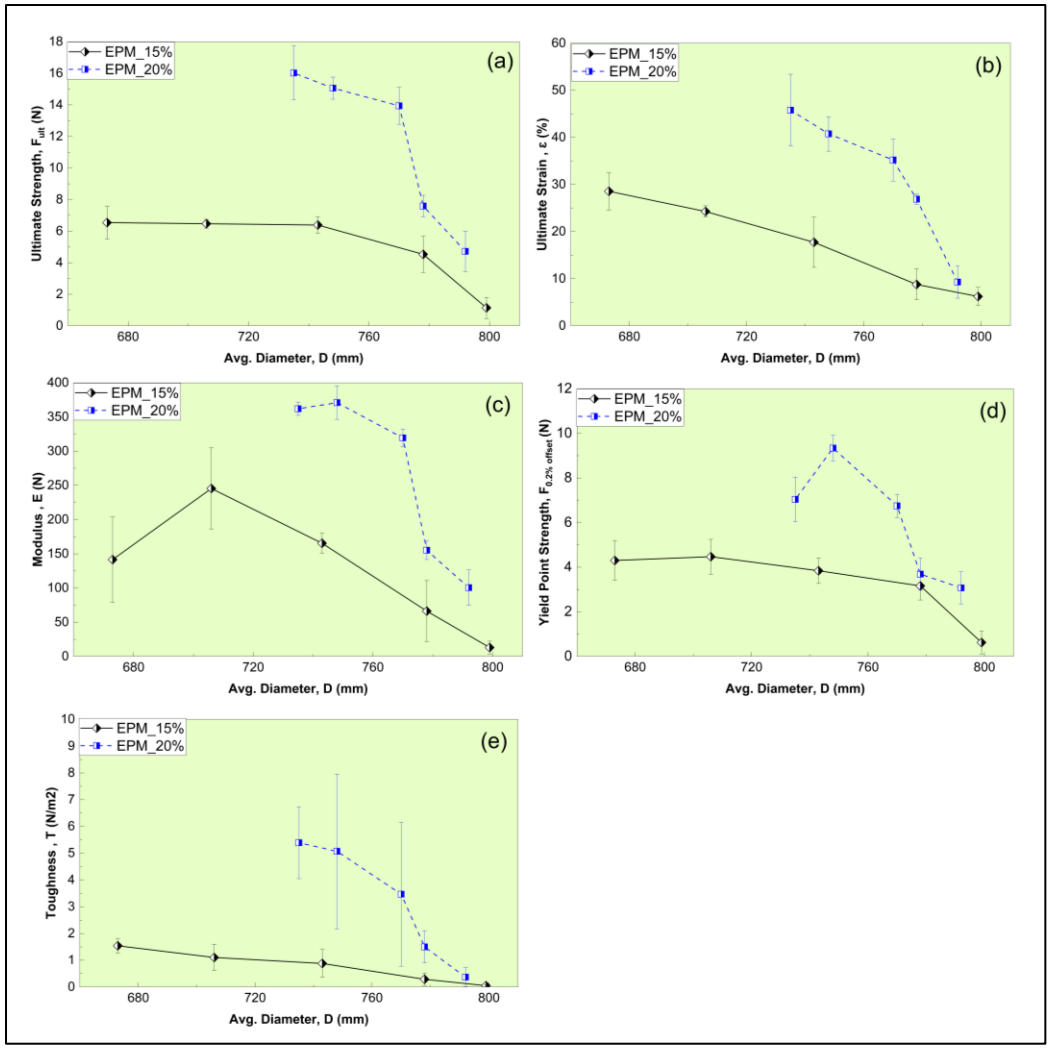

Figure 4.7 Mechanical properties EPM from two PET concentration of five different discharge rates with respect to fiber diameters (a) Ultimate Strength, F_{ult} (b) Ultimate Strain, ε (c) Modulus, E (d) Yield Strength at 0.2% offset, $F_{0.2\%\ offset}$ and (e) Toughness, T

A similar trend was also observed for EPM prepared by solutions having 20% PET concentration. In this case, the force corresponding to ultimate strength dropped from 16.02 N to 4.72 N as the fiber diameter changed from 735 nm to 792 nm (Figure 4.7a). In addition, the ultimate strain was found to decline from 28.6 % to 6.2% for a PET concentration of 15% as the fiber diameter increased from 673 nm to 799 nm. A similar trend was also observed for EPM prepared by solutions having 20% PET concentration. In this case, the strain corresponding to ultimate strength dropped from 48.36 % to 14.86 % as the fiber

diameter changed from 735 nm to 792 nm (Figure 4.7b). It was observed that the force corresponding to the ultimate strength and strain for the same discharge rates were higher when a concentration of 20% PET was used compared to EPMs produced using solutions having 15% PET concentration.

The modulus of EPM was found to increase from 13.02 N to 245.48 N for a PET concentration of 15% as the fiber diameter decreased from 799 to 706 nm. However, upon further reduction in diameter to 673 nm, the EPM's modulus decreased to 141.46 N. A similar trend was also observed for EPM prepared by solutions having 20% PET concentration. In this case, the modulus increased from 100.54 N to 370.88 N as the fiber diameter changed from 792 nm to 746 nm. Nevertheless, a subsequent reduction in diameter to 735 nm led to a decline in modulus to 361.94 N (Figure 4.7c). Interestingly, the highest modulus and force corresponding to yield strength values did not show a dependency on the fibers' diameters. For example, the modulus and force values corresponding to the yield point measured for the fibers produced with the PET concentration of 15%, increased by 74 and 4 %, respectively, as a result of increasing the fiber diameter from 673 to 706 nm. Continuing to raise the diameter of the fiber from 706 to 799 nm resulted in a reduction in both modulus and yield force values by 95 and 86 %, respectively (Figure 4.7c and 4.7d). For EPMs produced using solutions of 20% PET concentration, an increase in fiber diameters from 735 nm to 748 nm was associated with an increase in modulus and yield force. However, as the diameter further changed from 746 nm to 792 nm, both modulus and ultimate strain values exhibited a decreasing trend. Despite showing similar variation patterns of modulus and ultimate strain values with fiber diameters in both PET concentrations, fibers produced using 20% PET concentration

showed higher modulus and ultimate strain values compared to those produced with solutions of 15% PET concentration.

Figure 4.7e shows the variation of toughness values and fiber diameters. It was observed that the toughness values decreased with increasing the fiber diameters. More specifically, the fibers produced with a solution of 15% PET concentration showed to decrease by 97 % as a result of increasing the fiber diameter from 673 to 799 nm. A similar trend was also observed for EPM prepared by solutions having 20% PET concentration. In this case, toughness values dropped by 93% as the fiber diameter changed from 735 nm to 792 nm (Figure 4.7e) Therefore, fibers produced with 20% PET concentration are expected to have a higher energy absorption before fracture than those produced with 15%. PET concentration. The changes in observed mechanical properties of EPM can be attributed to the ultrafine nanofibers' interconnected chain orientation network and uniform distribution of the fibers' internal structure as fibers get finer (Papkov et al., 2013).

Reviewing the presented mechanical properties of the EPMs produced in the laboratory reveals that the highest modulus and strength values were achieved when the fibers were produced by electrospinning of a solution of 20% PET concentration at a discharge rate of 50 μL/min. While smoother and more uniform fibers were achieved by electrospinning PET solutions discharge rates below 50 μL/min, a significant drop in their diameter decreased substantially, resulting in a reduction in the force corresponding to yield point and a more pronounced plastic behavior. However, as the discharge rate decreased, the produced fibers became finer and more cylindrical, resulting in enhanced mechanical properties. Consequently, at reduced discharge rates, the ultimate strength and toughness increased.

CHAPTER FIVE: TEST RESULTS OF ASPHALT MIXES

5.1. Introduction

Four different types of asphalt mixes, containing 0, 0.5, 1.0, and 1.5% EPM, labeled as HMA-C, HMA + 0.5% EPM, HMA + 1.0% EPM, and HMA + 1.5% EPM were produced in the laboratory. The effect of incorporating different amounts of EPM in the HMA mixes on their resistance to different distresses was evaluated by conducting performance tests on the aforementioned mixes. This chapter summarizes performance of the asphalt mixes and their resistance to rutting, cracking, and moisture-induced damage by conducting HWT, SCB, and TSR tests, respectively.

5.2. Hamburg Wheel Tracking (HWT) Test Results

In this study, the rutting and moisture susceptibility of asphalt mixes containing different amounts of EPM were evaluated by conducting the HWT test in accordance with the AASHTO T 324 standard test method (AASHTO, 2011). HWT device automatically records rut depths at 11 equally-space locations on the wheel path during each wheel pass in the laboratory. For each HMA mix, two sets of identical specimens (four cylindrical samples) were prepared and tested in an HWT device. Tests were conducted at 50ºC while specimens were submerged in the water. After completing each HWT test, the measured rut depth was plotted with the number of wheel passes and used to analyze the rutting behavior of each mix. The deformation-wheel pass plot provides valuable insight into the performance of the asphalt pavement and demonstrates three distinct phases: post-compaction, creep, and stripping phases (Al-Khateeb and Basheer, 2009; Lv et al., 2018 and Zhang et al., 2020). Figures 2.1 and 2.2 in section 2.6.1 illustrate the characteristics of

the three phases of deformation associated with the rutting curve. The post-compaction phase corresponds to the consolidation of the specimen as the asphalt mix is compacted under the wheel load. The principal mechanism of deformation is the compaction of the mix caused by the applied load. The creep phase is characterized predominantly by the viscous flow of asphalt mixes. This phase is characterized by a creep slope, which represents a constant rate of rut depth per load cycle. The viscous behavior of asphalt mixes is responsible for permanent deformation during the creep phase. On the other hand, the stripping phase begins when the bond between the asphalt binder and aggregate weakens, which results in visible damage to the asphalt mix structure manifested by a dramatic increase in creep slope. To distinguish the stripping phase from the creep phase, another parameter called stripping inflection point (SIP) is utilized. During the stripping phase, the rate of rutting depth increase is typically double that of the creep phase (Lin et al., 2023).

Figure 5.1 shows the variation of rut depths with wheel passes obtained from conducting HWT tests on HMA-C, HMA + 0.5% EPM, HMA + 1.0% EPM, and HMA + 1.5% EPM mixes. Based on the results depicted in Figure 5.1, all the HMA mixes exhibited only post-compaction consolidation and creep, and none of them exhibited an SIP, indicating an adequate resistance to moisture-induced damage. The post-compaction consolidation was ended when the wheel passes reached approximately 3500, 3000, 2500, and 4000 loading cycles for HMA-C, HMA + 0.5% EPM, HMA + 1.0% EPM, and HMA + 1.5% EPM mixes, respectively. It is worth noting that the addition of EPM to the mix reduced the post-compaction phase, meaning that fewer loading cycles are required to transition into the creep phase. This observation indicates that EPM fibers can reduce the post-compaction consolidation of the HMA, resulting in delaying early deformations.

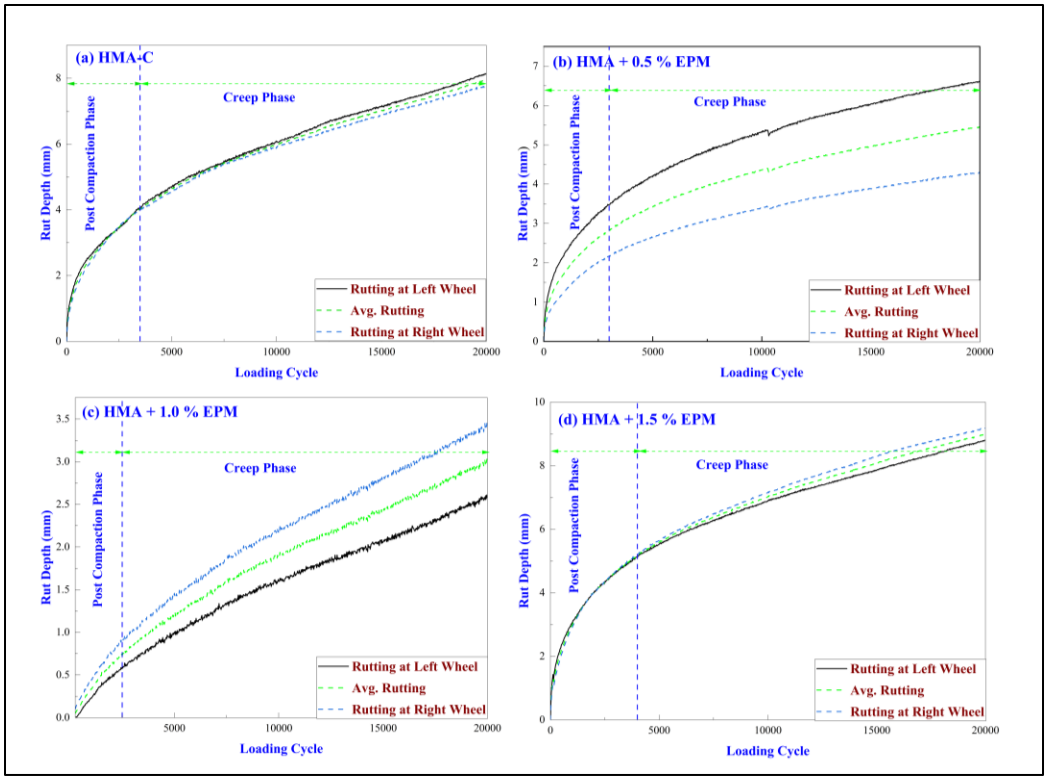

Figure 5.1 Rutting development in different EPM added HMA

Following the post-compaction phase, an extended and well-defined creep phase was observed, which continued for the remaining 20,000 loading cycles until the end of the test. Notably, a significant stripping phase was not evident. This observation suggests that the addition of the EPM did not compromise the asphalt-binder aggregate bonding and effectively resisted the stripping. Throughout the entire 20,000 loading cycles, the rutting depths of all HMA samples remained well below 12.5 mm, the maximum allowable rut depths for many DOTs. It was observed that asphalt mixes containing 0.5% and 1.0% EPM effectively reduced the maximum rut depths compared to the HMA-C. However, when the EPM content was increased to 1.5%, the maximum recorded rut depth increased and became similar to those observed in HMA-C. Table 5.1 summarizes the creep slope values and rut depths measured at 5000-wheel pass intervals for the tested mixes. It was observed that the rut depths for HMA-C, which does not contain any EPM, were 4.6, 6.0, 7.0, and

7.9 mm at 5000, 10,000, 15,000 and 20,000 wheel passes, respectively. The results indicate that HMA-C had a creep slope of 5,196 passes/mm, implying that it requires a minimum of 5,000 loading cycles to accumulate one mm of rutting.

Table 5.1 Summary of rut depths and creep slope for different mixes

SL No	Mix Type	Value	Rut depth (mm) No. passes				Inverse Creep Slope (Passes/mm)
			5,000	10,000	15,000	20,000	
1	HMA-C	Avg. L	4.7	6.1	7.1	8.1	5390
		Avg. R	4.6	5.9	6.9	7.8	5002
		Avg	4.6	6.0	7.0	7.9	5196
		SD	0.1	0.1	0.2	0.3	274
2	HMA + 0.5% EPM	Avg. L	2.6	3.4	3.9	4.3	10,904
		Avg. R	4.2	5.3	6.0	6.6	7622
		Avg	3.4	4.4	5.0	5.5	9263
		SD	1.1	1.4	1.5	1.6	2321
3	HMA + 1.0% EPM	Avg. L	1.0	1.6	2.1	2.6	10,362
		Avg. R	1.5	2.2	2.8	3.4	8172
		Avg	1.2	1.9	2.4	3.0	9267
		SD	0.3	0.4	0.5	0.6	1549
4	HMA + 1.5% EPM	Avg. L	5.5	6.9	7.9	8.8	5273
		Avg. R	5.6	7.2	8.3	9.2	4935
		Avg	5.6	7.0	8.1	9.0	5104
		SD	0.1	0.2	0.3	0.3	239

In contrast, the measured rut depths for HMA + 0.5% EPM at 5000, 10000, 15000, and 20,000 loading cycles were 3.4, 4.4, 5.0, and 5.5 mm, respectively. This indicates that adding 0.5% EPM to the asphalt mix significantly enhanced its resistance to rutting compared to HMA-C. The creep slope of 9,263 passes/mm recorded for HMA + 0.5% EPM indicates more than 78% improvement in resistance to rutting as a result of using 0.5% EPM compared to HMA-C. Furthermore, the rut depths recorded for HMA + 1.0% EPM mix after 5000, 10000, 15000, and 20000 wheel passes were 1.2, 1.9, 2.4, and 3.0 mm, respectively. The creep slope measured for the HMA + 1.0% EPM mix was 9,267 passes/mm. This indicates that the HMA containing 1.0% EPM, by weight of the asphalt binder, experienced a progression in rutting, which was approximately 78% slower than

that in HMA-C. This improvement in rutting resistance can be attributed to the important role played by EPM and the aggregate skeleton in the mix, including effective load distribution, particle interlock, reduced binder viscosity, reduced tensile and shar deformation due to the fibers and increased binder stiffness.

The HMA + 1.5% EPM mix exhibited rut depths of 5.6, 7.0, 8.1, and 9.0 mm at 5000, 10000, 15000, and 20000 wheel passes, respectively. Additionally, the creep slope measured for HMA + 1.5% EPM was 5,104 passes/mm, which indicated that the mixture containing 1.5% EPM rutted at a rate similar to that in HMA-C. This change in creep slope is attributed to the asphalt binder film thickness on aggregates and EPM. Since the binder content in all batches of asphalt mixes remained unchanged, the addition of EPM increased the available surface to be coated by asphalt, a reduction in asphalt film thickness. On the other hand, the addition of EPM increased the mixture's overall stiffness by reducing the ductility of the mastic. Finally, more EPM means more binder absorption and less effective binder content (P_{be}) less binder to coat the aggregates. As a result, at low EPM contents (0.5 and 1.0%), asphalt mixes exhibited a rutting resistance higher than that of the HMA-C. However, when the EPM content was increased to 1.5% asphalt mix showed a resistance to rutting approximately equal to that of the HMA-C. In addition, the absence of stripping inflection points (SIP) in Figure 5.1 indicates that none of the four mixes, including the control mixture, exhibited moisture-induced damage during the test. Consequently, SIP values were not reported in Table 5.1.

Figure 5.2 summarizes the maximum average rut depths of different tested HMA samples. The results indicated that for EPM contents less than 1.5%, an increase in the EPM contents resulted in a reduction in average rut depths when compared to HMA-C.

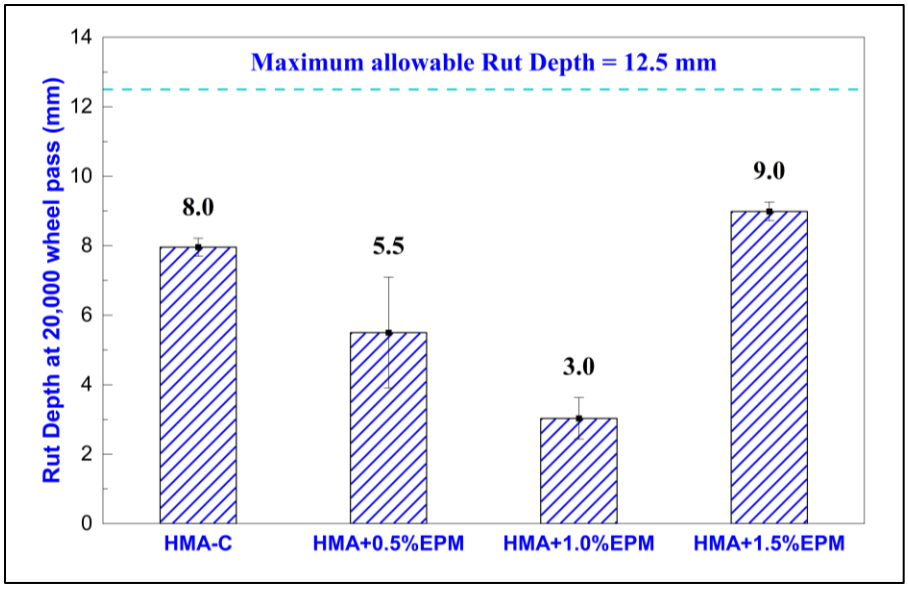

Figure 5.2 Maximum rut depths measured in different mixes

This indicates 30 and 62% reduction in rut depths when 0.5 and 1.0% EPM was incorporated in the mix, respectively, comparison to the HMA-C. As the EPM content reached 1.5%, observed ruth depth increased by 14% when compared to HMA-C.

5.3. Tensile Strength Ratio Test Results

The ITS tests were conducted on dry and moisture-conditioned samples to determine the moisture-induced damage potential in asphalt. For this purpose, one group of the specimens was subjected to moisture-conditioning by vacuum-saturating them with water, freezing at -18°C for 16 hours, and subjecting them to 60°C in a water bath for 24 hours. Finally, samples were kept submerged in the water at 25°C for two hours before testing. Another set of the samples (dry set) was kept at 25°C for two hours in dry condition before testing. A monotonic load was then applied to both sets of samples along their diameter in an ITS jig inside a loading frame. The average tensile strength of each sample set was then calculated by measuring the peak load from equation 3.2. The TSR value was then calculated for each mix type from equation 3.3.

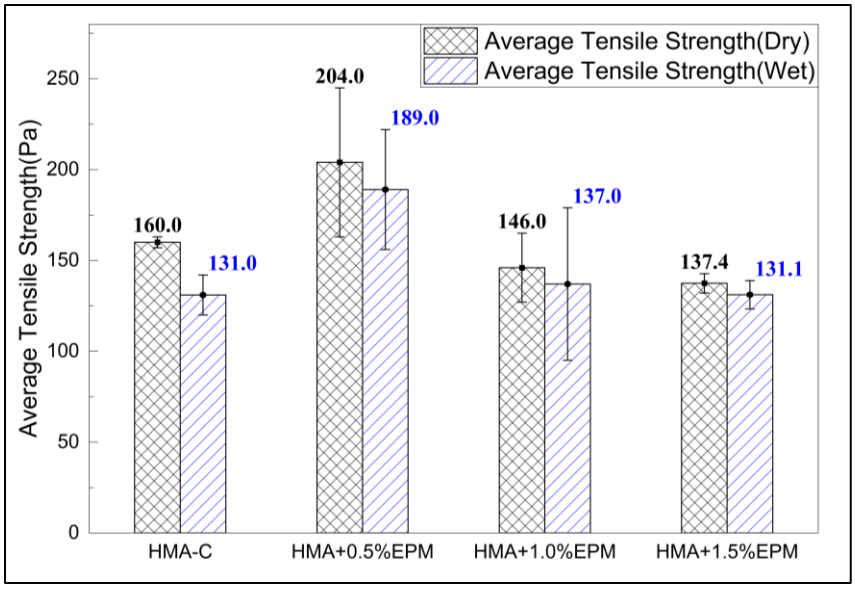

Figure 5.3 Tensile strength values of asphalt mixes in dry and moisture-conditioned states

Figure 5.3 shows the average tensile strength values for dry set and conditioned set for each type of the tested mixes. The TSR values calculated for each mix type are also shown in Figure 5.4. It was observed that the average tensile strength of dry-conditioned and moisture-conditioned HMA-C samples were 160.0 and 131.0 Pa, respectively, a TSR value of 81.8%. After adding 0.5% EPM to the asphalt mixes, the average tensile strength of the dry and moisture-conditioned samples rose to 204.0 and 189.0 Pa, respectively, a TSR value of 92.7%. This indicates that incorporating 0.5% EPM in asphalt mixes resulted in a 28 and 44% increase in the tensile strength of mixes in dry and wet conditions compared to those in the HMA-C mix, respectively. The EPM with a tensile strength higher than that of asphalt binder at 25ºC improved the tensile strength of asphalt mastic as a reinforced composite when compared to that of the HMA-C. It was observed that a further increase in the EPM content in the asphalt mixes (HMA + 1.0% EPM and HMA + 1.5% EPM) resulted in a reduction in tensile strengths of both dry and moisture-conditioned samples compared to HMA-C. More specifically, incorporating 1.0 and 1.5% EPM in the

mix resulted in 9 and 14% reduction in tensile strength of dry specimens, respectively, compared to HMA-C. However, the tensile strength of the moisture-conditioned samples containing 1.0 and 1.5% EPM remained unchanged, compared to that of the HMA-C.

According to Zhu et al. (2020) optimum asphalt binder content of asphalt mix increases after adding fibers which are directly related to the asphalt film thickness. Consequently, further addition of EPM led to reduction of the film thickness surrounding the aggregates and fibers. This occurred because more binder was required to coat the fibers, while binder content was kept constant in all mixes. Therefore, while the addition of EPM fibers beyond 0.5% had a negative effect on the tensile strength of samples tested in dry conditions, their presence was advantageous in reducing moisture damage to the mixture. This was observed through the fact that the tensile strength of the moisture-conditioned samples of the HMA containing 1.0 and 1,5% EPM remained unchanged compared to that of the HMA-C.

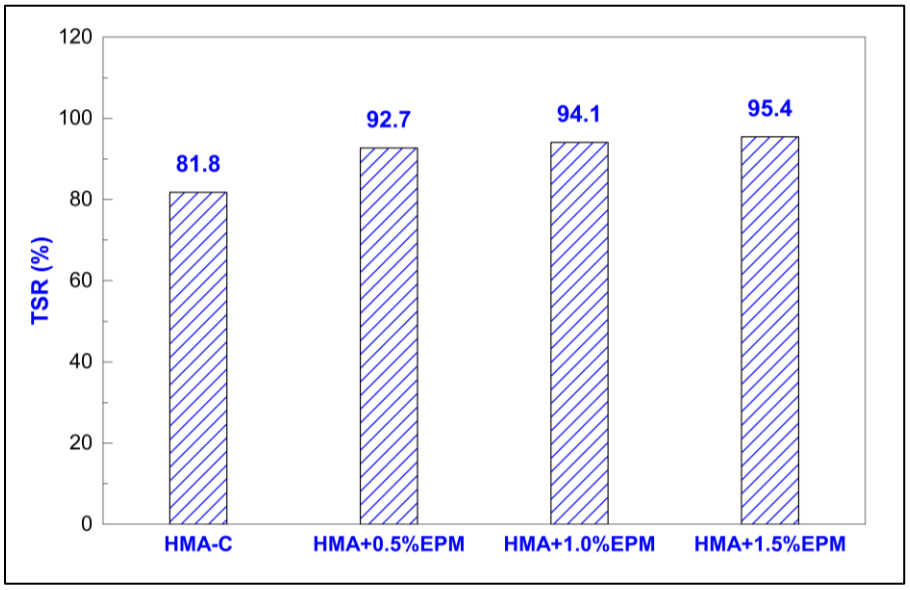

Figure 5.4 TSR result for different HMA mixes.

Figure 5.4 shows that the TSR values measured for HMA-C, HMA + 0.5% EPM, HMA + 1.0% EPM, and HMA + 1.5% EPM were 81.8, 92.7, 94.1, and 95.4%, respectively. It can be concluded that incorporating EPM into the HMA mix increased their resistance to moisture-induced damage. Interestingly, the continuous incorporation of EPM into asphalt mixes resulted in a continuous rise in TSR values compared to HMA-C. Therefore, one may conclude that the incorporation of the EPM in asphalt mixes can improve their resistance to moisture-induced damage.

5.4. Semi-Circular Bending (SCB) Test Results

Fatigue cracking is a frequently observed distress in asphalt pavements at intermediate temperatures. The SCB test was utilized to determine the resistance of the mixes to cracking (Klinsky et al., 2018). In addition, the fracture energy parameters obtained from conducting the SCB tests are found to have an excellent correlation with asphalt pavements' fatigue performance under repetitive traffic loads (Kim et al., 2012; Mohammad et al., 2008). Load-deformation curves developed by conducting the SCB test are analyzed to determine the critical strain energy release rate (J_c) from equation 3.1. Total energy represented by the area under the load-deformation up to the peak load corresponds to the crack initiation energy. By conducting SCB test on samples of different notch depth sensitivity of the crack initiation energy to notch depth is calculated for unit thickness of the sample, providing insight into asphalt material's crack resistance (Saha and Billigiri, 2016; Minhajuddin et al., 2016). To evaluate the resistance to cracking at intermediate temperature, fracture tests were conducted on SCB specimens having 25, 32, and 38 mm notch depths at 19°C. In each notch depth, at least four samples were tested. For each notch depth, the fracture energies were calculated. Figure 5.5 presents the critical strain energy

release rate (Jc) values for different asphalt mixes, namely HMA-C, HMA + 0.5% EPM, HMA + 1.0% EPM, and HMA + 1.5% EPM. It can be observed that incorporating of 0.5% EPM in asphalt mix resulted in 10% increase in the J_c value (0.44 kJ/m2). Compared to that of the HMA-C (0.4 kJ/m2). Similarly, the J_c value for the HMA + 1.0% EPM mix (0.58 kJ/m^2) was 45% higher than that of the HMA-C. Furthermore, incorporating 1.5% EPM in the mix resulted in 66% increase in J_c value (0.66 kJ/m^2) compared to HMA-C mix. This observation indicates that incorporation of EPM in asphalt mixes improved their resistance to cracking.

This enhancement in resistance to cracking was attributable to the fibers' capacity to absorb and distribute the concentrated tension generated by loading. Due to their greater energy absorption capacity compared to the asphalt binder and mastic phases, the presence of EPM contributes to delaying the microcrack formation (Ye et al., 2009).

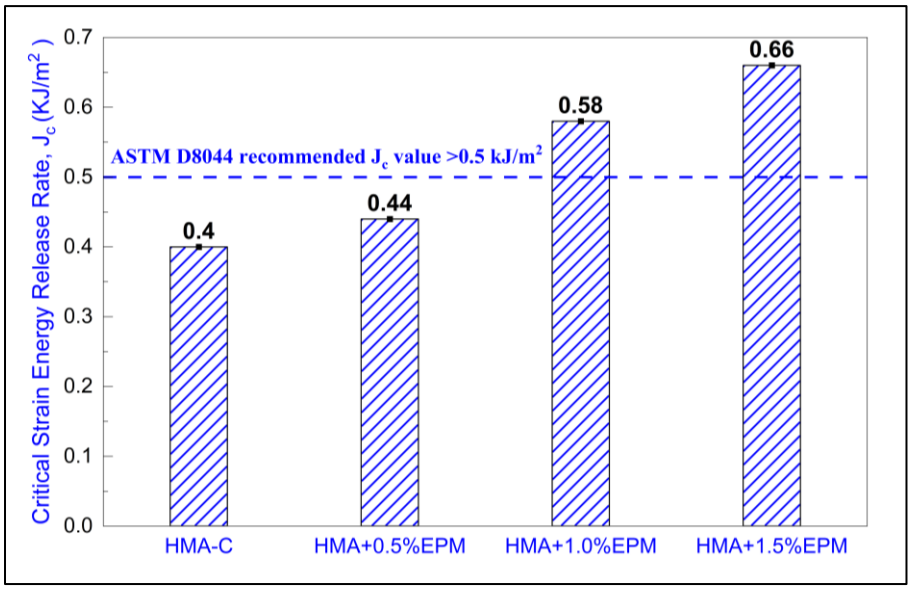

Figure 5.5 Critical Strain energy release rate (J_c) of different HMA mixes

Notably, ASTM D8044 (ASTM, 2017) recommends a minimum J_c value of 0.5 kJ/m^2 for an acceptable resistance to cracking. Figure 5.5 demonstrates that the measured

J_c values for HMA-C (0.40 kJ/m^2) and HMA + 0.5% EPM (0.44 kJ/m^2) were below this recommended threshold. However, addition of 1.0 and 1.5% EPM effectively increased the J_c values exceeding the minimum recommended threshold. This indicates that the addition of 1.0 and 1.5 % EPM can be considered as an effective method to improve asphalt mixes' resistance to cracking to meet the requirements of ASTM D8044 (ASTM, 2017).

CHAPTER SIX: CONCLUSIONS AND RECOMMENDATIONS

In this study, the production of the EPM in the laboratory by varying different concentrations and discharge rates were achieved. Also, the effect of the electrospinning parameters on the morphology and mechanical properties of the PET fibers were evaluated. The investigation involved the production of EPM using solution-based electrospinning techniques, employing different PET concentrations and discharge rates. The chemical, morphological, and mechanical properties of the EPM at different concentrations and discharge rates were assessed using FTIR, SEM, and tensile strength testing. In addition, laboratory produced Superpave mixes were prepared using a PG 58-28 asphalt binder and its blends with 0.5, 1.0, and 1.5% EPM. The effect of incorporating different amounts of EPM on resistance of the asphalt mixes to fatigue cracking, rutting and moisture-induced damage of asphalt mixes was characterized by conducting SCB, HWT, and TSR tests, respectively.

6.1. Conclusions

Based on the results, discussions, and observations presented in this study conclusions were drawn as follows.

a) Chemical analysis of EPMs using FTIR spectroscopy indicated that there were no significant alterations in the molecular structure of PET as a result of using the DCM and TFA solution and the electrospinning process. Also, no traces of DCM of TFA or additional functional groups were found in any of tested EPMs. It was further concluded

that drying of fibers in ventilated environment at room temperature for 24 hours is adequate for complete evaporation of the solvent.

b) From post-processing of the SEM micrographs, it was found that reducing the solution discharge rate led to a reduction in the fiber diameter. Higher PET concentrations in electrospinning solution resulted in fibers with larger diameters.

c) Qualitative study of the SEM micrographs revealed that regardless of the PET concentration in the solution the fibers with the highest degree of uniformity were consistently generated at the lowest spinnable discharge rate. Increasing the discharge rates resulted in rough, non-uniform and fractured fibers. For 15% PET concentration, uniform, smooth surface and cylindrical EPMs were produced at discharge rates less than 60 µL/min. For PET concentration of 20%, uniform, smooth surface and cylindrical EPMs were produced at discharge rates less than 120 µL/min.

d) Conducting tensile tests on EPMs revealed that a reduction in the diameter of the produced EPM resulted in an improvement in the strength, force corresponding to the yield point, and modulus of the fibers.

e) Based on chemical, morphological, and mechanical characteristics, as well as the requirements for mass production of EPMs, it was determined that utilizing a solution with a PET concentration of 20% and a discharge rate of 60 µL/min led to the production of EPMs exhibiting optimal mechanical properties. These attributes included exceptional tensile strength, strain, yield point strength, and toughness.

f) Based on the results of HWT tests, increasing the EPM content in the mix up to 1.0% resulted in continuous improvement in their resistance to rutting and moisture-induced damage compared to the mix without any fibers in it. However, further increase in EPM

content in the mix to 1.5% was found to have a negative effect on resistance of the mix to rutting compared to the mix without any fibers in it (HMA-C).

g) TSR values suggested that addition of EPM to asphalt mix increased the TSR value, an improved resistance to moisture-induced damage.

h) The SCB tests indicated that an increase in the EPM contents in the asphalt mixes tested in this study continuously improved their resistance to cracking, when compared to control mix.

i) Based on HWT, SCB, TSR as well as the requirements for mass uses of EPMs in asphalt mix, it was determined that utilizing 1.0% EPMs led to the performance of optimal mechanical properties of asphalt mix.

6.2. Recommendations

a) For future studies, it is recommended to explore and evaluate different methods of electrospinning EPM, with a particular focus on techniques such as melting electrospinning. This alternative method can eliminate the need for chemicals. Additionally, investigating different techniques for enhancing fiber production, such as experimenting with various solvents and their ratios, are suggested to be considered. These efforts would contribute to advancing the production process and expanding the range of applications for EPM fibers.

b) For improved control over the morphology of EPM fibers, it is recommended to optimize a number of environmental factors. In the beginning of the electrospinning, the discharge rate must be carefully regulated. The diameter and uniformity of the produced fibers can be substantially altered by adjusting the discharge rate. Secondly, it is essential to maintain a controlled humidity level in the laboratory. Fluctuations in

humidity can influence the electrospinning procedure and result in morphological variations in the fibers. During the electrospinning procedure, it is essential to maintain a stable and regulated humidity level. Dispersing the solution horizontally onto the collection plate was studied in this work. For future studies, exploring vertical discharge is suggested. During the electrospinning process, when the solution is discharged horizontally, it may take different travel trajectories. Consequently, the morphology of electrospun fibers may vary along the collection plate. By electrospinning of the solution vertically, it is possible to achieve a more consistent and controlled travel path, resulting in enhanced fiber morphology.

c) As a result of the use of highly polarized solvents in the production of EPM fibers, the surfaces of the fibers tend to be highly charged. To mitigate this issue, it is recommended to investigate alternative electrospinning techniques that can aid in lowering the surface charge of EPM fibers. By employing these alternative techniques, it may be possible to achieve a more balanced surface charge distribution, resulting in enhanced dispersion in asphalt.

d) Before the proposed modified asphalt can be adopted as a standard construction material in pavements, additional field-scale construction, long-term pavement performance monitoring and life cycle cost analysis (LCCA) should be conducted. The conclusions regarding mix performance were derived from tests conducted on a specific mix design that included local aggregates, a particular grading, and other site-specific variables. These results may not be directly applicable to other mixes or material varieties. To further expand the applicability of the findings, further research should be carried out to

include a variety of materials. This would entail testing the asphalt binders and different aggregate sources, aggregate gradations, and other mix variables.

Reference

AASHTO (2011). Standard Specification for Transportation Materials and Methods of Sampling and Testing. 31st edition. American Association of State Highway and Transportation Officials (AASHTO), Washington, DC.

Abbas, J. A., Said, I. A., Mohamed, M. A., Yasin, S. A., Ali, Z. A., and Ahmed, I. H. (2018, December). Electrospinning of polyethylene terephthalate (PET) nanofibers: Optimization study using taguchi design of experiment. In IOP conference series: materials science and engineering (Vol. 454, No. 1, p. 012130). IOP Publishing.

Abtahi, S. M., Sheikhzadeh, M., and Hejazi, S. M. (2010). Fiber-reinforced asphalt-concrete–a review. Construction and Building Materials, 24(6), 871-877.

Afonso, M. L., Dinis-Almeida, M., and Fael, C. S. (2017). Study of the porous asphalt performance with cellulosic fibres. Construction and Building Materials, 135, 104-111.

Ahmadinia, E., Zargar, M., Karim, M. R., Abdelaziz, M., and Ahmadinia, E. (2012). Performance evaluation of utilization of waste Polyethylene Terephthalate (PET) in stone mastic asphalt. Construction and Building Materials, 36, 984-989.

Alfalah, A., Offenbacker, D., Ali, A., Decarlo, C., Lein, W., Mehta, Y., and Elshaer, M. (2020). Assessment of the impact of fiber types on the performance of fiber-reinforced hot mix asphalt. Transportation Research Record, 2674(4), 337-347.

Ali, B., Qureshi, L. A., & Khan, S. U. (2020). Flexural behavior of glass fiber-reinforced recycled aggregate concrete and its impact on the cost and carbon footprint of concrete pavement. Construction and Building Materials, 262, 120820.

Al-Khateeb, G., and Basheer, I. (2009). A three-stage rutting model utilising rutting performance data from the Hamburg Wheel-Tracking Device (WTD). Road and Transport Research: A Journal of Australian and New Zealand Research and Practice, 18(3), 12-25.

Al-Qadi, I. L., Ozer, H., Lambros, J., El Khatib, A., Singhvi, P., Khan, T., Rivera, J., and Doll, B. (2015). Testing Protocols to Ensure Performance of High Asphalt Binder Replacement Mixes Using RAP and RAS. A report of the findings of ICT-R27-128. Illinois Center for Transportation Series No. 15-017. Research Report No. FHWA-ICT-15-017. Illinois Center for Transportation.

Alshamsi, K. S. (2006). Development of a mix design methodology for asphalt mixtures with analytically formulated aggregate structures. Louisiana State University and Agricultural & Mechanical College.

Aschenbrener, T., and Currier, G. (1993). Influence of Testing Variables on The Results from The Hamburg Wheel-Tracking Device. FINAL REPORT (No. CDOT-DTD-R-93-22).

ASTM D 3822, (2007). Standard Test Method for Tensile Properties of Single Textile Fiber, ASTM International, West Conshohocken, PA.

ASTM D 8044, (2017). Standard Test Method for Evaluation of Asphalt Mixture Cracking Resistance using the Semi-Circular Bend Test (SCB) at Intermediate Temperatures, ASTM International, West Conshohocken, PA.

ASTM D 882, (2018). Standard Test Method for Tensile Properties of Thin Plastic Sheeting, ASTM International, West Conshohocken, PA.

Aydemir, H., and Demiryürek, O. (2022). The effect of electrospinning parameters on morphology and diameter of polyethylene terephthalate (PET) and recycled polyethylene terephthalate (r-PET) nanofibers. The Journal of The Textile Institute, 1-12.

Bagampadde, U., Isacsson, U., and Kiggundu, B. M. (2006). Impact of bitumen and aggregate composition on stripping in bituminous mixtures. Materials and structures, 39, 303-315.

Behnood, A., and Gharehveran, M. M. (2019). Morphology, rheology, and physical properties of polymer-modified asphalt binders. European Polymer Journal, 112, 766-791.

Ben Zair, M. M., Jakarni, F. M., Muniandy, R., and Hassim, S. (2021). A brief review: application of recycled polyethylene terephthalate in asphalt pavement reinforcement. Sustainability, 13(3), 1303.

Beyler, C. L., and Hirschler, M. M. (2002). Thermal decomposition of polymers. SFPE handbook of fire protection engineering, 2(7).

Bhasin, A. (2007). Development of methods to quantify bitumen-aggregate adhesion and loss of adhesion due to water (Doctoral dissertation, Texas A and M University).

Bonfim, D. P., Cruz, F. G., Bretas, R. E., Guerra, V. G., and Aguiar, M. L. (2021). A sustainable recycling alternative: Electrospun PET-membranes for air nanofiltration. Polymers, 13(7), 1166.

Bozorgzad, A., Kazemi, S. F., and Nejad, F. M. (2018a). Finite-element modeling and laboratory validation of evaporation-induced moisture damage to asphalt mixtures. In Proceedings of the 97th transport research board annual meeting. Transportation Research Board, Washington, DC.

Bozorgzad, A., Kazemi, S. F., and Nejad, F. M. (2018b). Evaporation-induced moisture damage of asphalt mixtures: Microscale model and laboratory validation. Construction and Building Materials, 171, 697-707.

Breakah, T. M., and Williams, R. C. (2015). Stochastic finite element analysis of moisture damage in hot mix asphalt. Materials and Structures, 48, 93-106.

Chaturabong, P., and Bahia, H. U. (2017). The evaluation of relative effect of moisture in Hamburg wheel tracking test. Construction and Building Materials, 153, 337-345.

Chavan, S., and Rao, P. (2016). Utilization of Waste PET Bottle Fibers in Concrete as an Innovation in Building Materials— [A Review Paper]. Int. J. Eng. Res, 5(1), 304-307.

Chen, H. X., Li, N. L., Hu, C., and Zhang, Z. (2004). Mechanical performance of fibers-reinforced asphalt mixture. J Chan Univ (Nat Sci Ed), 24(2), 1-5.

Chen, H., and Xu, Q. (2010). Experimental study of fibers in stabilizing and reinforcing asphalt binder. Fuel, 89(7), 1616-1622.

Chen, J. S., and Lin, K. Y. (2005). Mechanism and behavior of bitumen strength reinforcement using fibers. Journal of materials science, 40, 87-95.

Chen, M. J., and Wong, Y. D. (2013). Porous asphalt mixture with 100% recycled concrete aggregate. Road Materials and Pavement Design, 14(4), 921-932.

Chen, M. J., and Wong, Y. D. (2015). Porous asphalt mixture with a combination of solid waste aggregates. Journal of Materials in Civil Engineering, 27(6), 04014194.

Chen, Z., Wu, S. P., Zhu, Z. H., and Liu, J. S. (2008). Experimental evaluation on high temperature rheological properties of various fiber modified asphalt binders. Journal of Central South University of Technology, 15, 135-139.

Cheng, M., Qin, Z., Hu, S., Yu, H., and Zhu, M. (2017). Use of electrospinning to directly fabricate three-dimensional nanofiber stacks of cellulose acetate under high relative humidity condition. Cellulose, 24(1), 219-229.

Cho, C. J., Chang, Y. S., Lin, Y. Z., Jiang, D. H., Chen, W. H., Lin, W. Y.,Chen, C.W., Rwei, S.P. and Kuo, C. C. (2020). Green electrospun nanofiber membranes filter prepared from novel biomass thermoplastic copolyester: Morphologies and filtration properties. Journal of the Taiwan Institute of Chemical Engineers, 106, 206-214.

Chong, K., and Kuruppu, M. D. (1984). New specimen for fracture toughness determination for rock and other materials. International Journal of Fracture, 26(2), R59–R62.

Christiansen, L., Gurevich, L., Wang, D., and Fojan, P. (2021). Melt Electrospinning of PET and Composite PET-Aerogel Fibers: An Experimental and Modeling Study. Materials, 14(16), 4699.

Coleri, E., Tsai, B. W., and Monismith, C. L. (2008). Pavement rutting performance prediction by integrated Weibull approach. Transportation research record, 2087(1), 120-130.

Cong, L., Peng, J., Guo, Z., and Wang, Q. (2017). Evaluation of fatigue cracking in asphalt mixtures based on surface energy. Journal of Materials in Civil Engineering, 29(3), D4015003.

Copeland, A. (2005). Moisture in asphalt pavements in the United States: A financial perspective. In First international workshop on moisture damage.

Copeland, A. (2011). Reclaimed asphalt pavement in asphalt mixtures: State of the practice (No. FHWA-HRT-11-021). United States. Federal Highway Administration. Office of Research, Development, and Technology.

Cramariuc, B., Cramariuc, R., Scarlet, R., Manea, L. R., Lupu, I. G., and Cramariuc, O. (2013). Fiber diameter in electrospinning process. Journal of Electrostatics, 71(3), 189-198.

Das, P. K., Baaj, H., Kringos, N., and Tighe, S. (2015). Coupling of oxidative ageing and moisture damage in asphalt mixtures. Road Materials and Pavement Design, 16(sup1), 265-279.

Dasdemir, M., Topalbekiroglu, M., and Demir, A. (2013). Electrospinning of thermoplastic polyurethane microfibers and nanofibers from polymer solution and melt. Journal of Applied Polymer Science, 127(3), 1901-1908.

Dhaka, V., Singh, S., Anil, A. G., Sunil Kumar Naik, T. S., Garg, S., Samuel, J., Kumar, M., Ramamurthy, P.C., and Singh, J. (2022). Occurrence, toxicity and remediation of polyethylene terephthalate plastics. A review. Environmental Chemistry Letters, 1-24.

Domingos, M. D. I., and Faxina, A. L. (2016). Susceptibility of asphalt binders to rutting literature review. Journal of Materials in Civil Engineering, 28(2), 04015134.

Doshi, J., and Reneker, D. H. (1995). Electrospinning process and applications of electrospun fibers. Journal of electrostatics, 35(2-3), 151-160.

Du, Y., Chen, J., Han, Z., and Liu, W. (2018). A review on solutions for improving rutting resistance of asphalt pavement and test methods. Construction and Building Materials, 168, 893-905.

Enieb, M., Diab, A., and Yang, X. (2021). Short-and long-term properties of glass fiber reinforced asphalt mixtures. International Journal of Pavement Engineering, 22(1), 64-76.

Espíndola-González, A., Martínez-Hernández, A. L., Fernández-Escobar, F., Castaño, V. M., Brostow, W., Datashvili, T., and Velasco-Santos, C. (2011). Natural-synthetic hybrid polymers developed via electrospinning: the effect of PET in chitosan/starch system. International journal of molecular sciences, 12(3), 1908-1920.

Fang, J., and Lin, T. (2019). Energy harvesting properties of electrospun nanofibers.

Faruk, A. N., Lee, S. I., Zhang, J., Naik, B., and Walubita, L. F. (2015). Measurement of HMA shear resistance potential in the lab: The Simple Punching Shear Test. Construction and Building Materials, 99, 62-72.

Freeman, R. D., Burati, J. L., Amirkhanian, S. N., and Bridges, W. C. (1989). Polyester fibers in asphalt paving mixtures. In Association of Asphalt Paving Technologists Proc (Vol. 58).

Ghabchi, R., Arshadi, A., Zaman, M., & March, F. (2021). Technical challenges of utilizing ground tire rubber in asphalt pavements in the united states. *Materials*, *14*(16), 4482.

Ghabchi, R. & Acharya, R. (2022). Evaluation of Fracture Energy Parameters for Predicting Moisture-Induced Damage in Asphalt Mixes. Transportation Infrastructure Geotechnology, 9(3), pp.356-384.

Ghabchi, R., & Castro, M. P. P. (2021). Effect of laboratory-produced cellulose nanofiber as an additive on performance of asphalt binders and mixes. Construction and Building Materials, 286, 122922.

Ghabchi, R., Dharmarathna, C. P., and Mihandoust, M. (2021). Feasibility of using micronized recycled Polyethylene Terephthalate (PET) as an asphalt binder additive: A laboratory study. Construction and Building Materials, 292, 123377.

Goel, A., & Das, A. (2004, August). Emerging road materials and innovative applications. In National conference on materials and their application in Civil Engg.

Großegger, D. (2016, June). Microstructural aging of bitumen. In Proceedings of the EE Congress 2016 6th EurasphaltEurobitume Congress, Prague, Czech Republic (pp. 1-3).

Haider, A., Haider, S., and Kang, I. K. (2018). A comprehensive review summarizing the effect of electrospinning parameters and potential applications of nanofibers in biomedical and biotechnology. Arabian Journal of Chemistry, 11(8), 1165-1188.

Hassan, H. F., Al-Oraimi, S., and Taha, R. (2005). Evaluation of open-graded friction course mixtures containing cellulose fibers and styrene butadiene rubber polymer. Journal of materials in civil engineering, 17(4), 416-422.

Hassani, A., Ganjidoust, H., and Maghanaki, A. A. (2005). Use of plastic waste (poly-ethylene terephthalate) in asphalt concrete mixture as aggregate replacement. Waste Management and Research, 23(4), 322-327.

He, S. S., Wei, M. Y., Liu, M. H., and Xue, W. L. (2015). Characterization of virgin and recycled poly (ethylene terephthalate) (PET) fibers. The Journal of the Textile Institute, 106(8), 800-806.

Hoffman, G.L. and Solaimanian, M. (2019). Asphalt mix performance testing for PAPA update. Presented at 2019 Pennsylvania Asphalt Pavement Association (PAPA) reginal technical meeting, Pennsylvania.

Hofman, R., Oosterbaan, B., Erkens, S. M. J. G., and van der Kooij, J. (2003, April). Semi-circular bending test to assess the resistance against crack growth. In 6th RILEM symposium on performance testing and evaluation of bituminous materials (pp. 257-263).

Hopewell, J., Dvorak, R., and Kosior, E. (2009). Plastics recycling: challenges and opportunities. Philosophical Transactions of the Royal Society B: Biological Sciences, 364(1526), 2115-2126.

Hu, X., Liu, S., Zhou, G., Huang, Y., Xie, Z., and Jing, X. (2014). Electrospinning of polymeric nanofibers for drug delivery applications. Journal of controlled release, 185, 12-21.

Huang, B., Li, G., and Mohammad, L. N. (2003). Analytical modeling and experimental study of tensile strength of asphalt concrete composite at low temperatures. Composites Part B: Engineering, 34(8), 705-714.

Huang, B., Shu, X., and Zuo, G. (2013). Using notched semicircular bending fatigue test to characterize fracture resistance of asphalt mixtures. Engineering Fracture Mechanics, 109, 78–88. https://doi.org/10.1016/j.engfracmech.2013.07.003.

Huang, H., and White, T. D. (1996). Dynamic properties of fiber-modified overlay mixture. Transportation Research Record, 1545(1), 98-104.

Huang, Y. H. (2004). Pavement analysis and design (Vol. 2, pp. 401-409). Upper Saddle River, NJ: Pearson Prentice Hall.

Infrared Spectroscopy Absorption Table. (2020, November 3). Chemistry LibreTexts. Retrieved August 6, 2023, from https://chem.libretexts.org/Ancillary_Materials/Reference/Reference_Tables/Spectroscopic_Reference_Tables/Infrared_Spectroscopy_Absorption_Table

Jung, J. W., Lee, C. L., Yu, S., and Kim, I. D. (2016). Electrospun nanofibers as a platform for advanced secondary batteries: a comprehensive review. Journal of materials chemistry A, 4(3), 703-750.

Júnior, J. L. L., Babadopulos, L. F., and Soares, J. B. (2019). Moisture-induced damage resistance, stiffness and fatigue life of asphalt mixtures with different aggregate-binder adhesion properties. Construction and building materials, 216, 166-175.

Karimi, M. M., Jahanbakhsh, H., Jahangiri, B., and Nejad, F. M. (2018). Induced heating-healing characterization of activated carbon modified asphalt concrete under microwave radiation. Construction and Building Materials, 178, 254-271.

Kassem, H. A., Saleh, N. F., Zalghout, A. A., and Chehab, G. R. (2018). Advanced characterization of asphalt concrete mixtures reinforced with synthetic fibers. Journal of Materials in Civil Engineering, 30(11), 04018307.

Khoonkari, M., Haghighi, A. H., Sefidbakht, Y., Shekoohi, K., and Ghaderian, A. (2015). Chemical recycling of PET wastes with different catalysts. International Journal of Polymer Science, 2015.

Kiggundu, B. M., and Roberts, F. L. (1988). Stripping in HMA mixtures: State-of-the-art and critical review of test methods. https://rosap.ntl.bts.gov/view/dot/13637/dot_13637_DS1.pdf

Kim, J. H., Yang, S. S., and Hudson, S. M. (2011). Comparison of the structure-property relationships for PTT and PET fibers spun at various take-up speeds. Fibers and Polymers, 12(6), 771-777.

Koenig, K., Beukenberg, K., Langensiepen, F., and Seide, G. (2019). A new prototype melt-electrospinning device for the production of biobased thermoplastic sub-microfibers and nanofibers. Biomaterials Research, 23(1), 1-12.

Koo, B. M., Kim, J. H. J., Kim, S. B., and Mun, S. (2014). Material and structural performance evaluations of Hwangtoh admixtures and recycled PET fiber-added eco-friendly concrete for CO2 emission reduction. Materials, 7(8), 5959-5981.

Kringos, N. (2007). Modeling of combined physical-mechanical moisture induced damage in asphaltic mixes (Vol. 68, No. 02).

Kumbargeri, Y. S., and Biligiri, K. P. (2016). Understanding aging behaviour of conventional asphalt binders used in India. Transportation Research Procedia, 17, 282-290.

Lasprilla-Botero, J., Alvarez-Lainez, M., and Lagaron, J. M. (2018). The influence of electrospinning parameters and solvent selection on the morphology and diameter of polyimide nanofibers. Materials Today Communications, 14, 1-9.

Lastra-González, P., Indacoechea-Vega, I., Calzada-Pérez, M. A., Vega-Zamanillo, Á., and Castro-Fresno, D. (2020). Assessment of induction heating in the performance of porous asphalt mixtures. Road Materials and Pavement Design, 21(8), 2302-2320.

Lastra-González, P., Indacoechea-Vega, I., Calzada-Pérez, M. A., Vega-Zamanillo, Á., & Castro-Fresno, D. (2020). Assessment of induction heating in the performance of porous asphalt mixtures. Road Materials and Pavement Design, 21(8), 2302-2320.

Lee, S. J., Rust, J. P., Hamouda, H., Kim, Y. R., and Borden, R. H. (2005). Fatigue cracking resistance of fiber-reinforced asphalt concrete. Textile Research Journal, 75(2), 123-128.

Leng, Z., Padhan, R. K., and Sreeram, A. (2018a). Production of a sustainable paving material through chemical recycling of waste PET into crumb rubber modified asphalt. Journal of cleaner production, 180, 682-688.

Leng, Z., Sreeram, A., Padhan, R. K., and Tan, Z. (2018b). Value-added application of waste PET based additives in bituminous mixtures containing high percentage of reclaimed asphalt pavement (RAP). Journal of cleaner Production, 196, 615-625.

Li, X., Liu, H., Wang, J., and Li, C. (2012). Preparation and properties of PET/SiO2 composite micro/nanofibers by a laser melt-electrospinning system. Journal of applied polymer science, 125(3), 2050-2055.

Limón-Covarrubias, P., Avalos Cueva, D., Valdés Vidal, G., Reyes Ortiz, O. J., Adame Hernández, R. O., and Galaviz González, J. R. (2019). Analysis of the behavior of SMA mixtures with different fillers through the semicircular bend (SCB) fracture test. Materials, 12(2), 288.

Lin, P., Liu, X., Ren, S., Xu, J., Li, Y., and Li, M. (2023). Effects of Bitumen Thickness on the Aging Behavior of High-Content Polymer-Modified Asphalt Mixture. Polymers, 15(10), 2325.

Liu, Q., Schlangen, E., van de Ven, M., and García, Á. (2010). Healing of porous asphalt concrete via induction heating. Road Materials and Pavement Design, 11(sup1), 527-542.

Liu, Z., Xing, M., Chen, S., He, R., and Cong, P. (2014). Influence of the chloride-based anti-freeze filler on the properties of asphalt mixtures. Construction and Building Materials, 51, 133-140.

Luo, D., Khater, A., Yue, Y., Abdelsalam, M., Zhang, Z., Li, Y., ... and Iseley, D. T. (2019). The performance of asphalt mixtures modified with lignin fiber and glass fiber: A review. Construction and Building Materials, 209, 377-387.

Lv, Q., Huang, W., Zheng, M., Sadek, H., Zhang, Y., and Yan, C. (2020). Influence of gradation on asphalt mix rutting resistance measured by Hamburg Wheel Tracking test. Construction and Building Materials, 238, 117674.

Ma, J., Yu, L., Chen, S., Chen, W., Wang, Y., Guang, S., Zhang, X., Lu, W., Wang, Y., and Bao, J. (2018). Structure–property evolution of poly (ethylene terephthalate) fibers in industrialized process under complex coupling of stress and temperature field. Macromolecules, 52(2), 565-574.

Mamlouk, M. S., and Zaniewski, J. P. (2006). Materials for civil and construction engineers. , , Pearson Prentice Hall (SBN-13: 978-0136110583).

Marchioni, M., and Becciu, G. (2015). Experimental results on permeable pavements in urban areas: A synthetic review. International Journal of Sustainable Development and Planning, 10(6), 806-817.

Maurer, D. A., and Malasheskie, G. J. (1989). Field performance of fabrics and fibers to retard reflective cracking. Geotextiles and Geomembranes, 8(3), 239-267.

McDaniel, R. S. (2001). Asphalt additives to control rutting and cracking. Purdue University.

Mercado, E. A. (2007). Influence of fundamental material properties and air void structure on moisture damage of asphalt mixes (Vol. 68, No. 06).

Mercante, L. A., Scagion, V. P., Migliorini, F. L., Mattoso, L. H., and Correa, D. S. (2017). Electrospinning-based (bio) sensors for food and agricultural applications: A review. TrAC Trends in Analytical Chemistry, 91, 91-103.

Merkel, D. R., Kuang, W., Malhotra, D., Petrossian, G., Zhong, L., Simmons, K. L., ... and Cosimbescu, L. (2020). Waste PET chemical processing to terephthalic amides and their effect on asphalt performance. ACS Sustainable Chemistry and Engineering, 8(14), 5615-5625.

Miao, Y., von Jouanne, A., and Yokochi, A. (2021). Current technologies in depolymerization process and the road ahead. Polymers, 13(3), 449.

Modarres, A., and Hamedi, H. (2014a). Developing laboratory fatigue and resilient modulus models for modified asphalt mixes with waste plastic bottles (PET). Construction and Building Materials, 68, 259-267.

Modarres, A., and Hamedi, H. (2014b). Effect of waste plastic bottles on the stiffness and fatigue properties of modified asphalt mixes. Materials and Design, 61, 8-15.

Moghaddam, T. B., Karim, M. R., and Syammaun, T. (2012). Dynamic properties of stone mastic asphalt mixtures containing waste plastic bottles. Construction and Building Materials, 34, 236-242.

Mohammad, L. N., Kim, M., and Elseifi, M. (2012). Characterization of asphalt mixture's fracture resistance using the semi-circular bending (SCB) test. In 7th RILEM

International Conference on Cracking in Pavements: Mechanisms, Modeling, Testing, Detection and Prevention Case Histories (pp. 1-10). Springer Netherlands.

Mohammadinia, A., Disfani, M. M., Narsilio, G. A., and Aye, L. (2018). Mechanical behaviour and load bearing mechanism of high porosity permeable pavements utilizing recycled tire aggregates. Construction and Building Materials, 168, 794-804.

Moon, B., Ledtje, P., and Williams, C. (2022). Evaluating effect of rejuvenators on high RAP mixtures through laboratory performance tests and construction of field test sections. Construction and Building Materials, 340, 127698.

Moreno-Navarro, F., Sol-Sánchez, M., García-Travé, G., and Rubio-Gámez, M. C. (2018). Fatigue cracking in asphalt mixtures: the effects of ageing and temperature. Road Materials and Pavement Design, 19(3), 561-570.

National Association for PET Container Resources (NAPCOR). 2019 PET Recycling Report. Last online access: March 1, 2023. Available through: https://napcor.com/wp-content/uploads/2021/03/NAPCOR_2019RateReport_FINAL_rev.pdf

National Association for PET Container Resources (NAPCOR). Report on Postconsumer PET Recycling Activity in 2018. Last online access: July 12, 2022. Available through: https://napcor.com/wp-content/uploads/2021/07/Postconsumer-PET-Recycling-Activity-in-2018.pdf

Nelson, P. K., Li, V. C., and Kamada, T. (2002). Fracture toughness of microfiber reinforced cement compositessmith. Journal of Materials in Civil Engineering, 14(5), 384-391.

Norouzi, A., Kim, D., and Richard Kim, Y. (2016). Numerical evaluation of pavement design parameters for the fatigue cracking and rutting performance of asphalt pavements. Materials and Structures, 49, 3619-3634.

Nsengiyumva, G., Kim, Y.-R., and You, T. (2015). Development of a Semicircular Bend (SCB) test method for performance testing of Nebraska asphalt mixtures. Nebraska Department of Transportation Research Reports, 171. https://digitalcommons.unl.edu/ndor/171.

Ogata, N., Shimada, N., Yamaguchi, S., Nakane, K., and Ogihara, T. (2007). Melt-electrospinning of poly (ethylene terephthalate) and polyalirate. Journal of Applied Polymer Science, 105(3), 1127-1132.

Oruç, Ş., Yılmaz, B., and Sancak, K. (2022). Characterization and rheological behavior of asphalt binder modified by a novel cyclic borate ester additive. Construction and Building Materials, 348, 128673.

Ouchterlony, F. (1990). Fracture toughness testing of rock with core-based specimens. Engineering Fracture Mechanics, 35(1-3), 351-366.

Owida, H. A., Moh'd, B. A. H., and Al Takrouri, M. (2022). Designing an Integrated Low-cost Electrospinning Device for Nanofibrous Scaffold Fabrication. HardwareX, 11, e00250.

P. Gable, Prof. (2022, September 3). Infrared Spectroscopy: Identifying Functional Groups. https://sites.science.oregonstate.edu. Retrieved April 8, 2023, from https://sites.science.oregonstate.edu/~gablek/CH335/Chapter10/IR.htm?fbclid=IwAR2u4P9Lr6oSJs_p_Q2o4ysaum6f9DYyOqfuopYQ6YIqpVYDWYW17ObGXLM

Papkov, D., Zou, Y., Andalib, M. N., Goponenko, A., Cheng, S. Z., and Dzenis, Y. A. (2013). Simultaneously strong and tough ultrafine continuous nanofibers. ACS nano, 7(4), 3324-3331.

Park, D. W., Seo, W. J., Kim, J., and Vo, H. V. (2017). Evaluation of moisture susceptibility of asphalt mixture using liquid anti-stripping agents. Construction and Building Materials, 144, 399 405.

Park, P., El-Tawil, S., Park, S. Y., & Naaman, A. E. (2015). Cracking resistance of fiber reinforced asphalt concrete at− 20 C. Construction and Building Materials, 81, 47-57.

Peltonen, P. (1991a). Wear and deformation characteristics of fibre reinforced asphalt pavements. Construction and building Materials, 5(1), 18-22.

Peltonen, P. V. (1991b). Characterization and testing of fibre-modified bitumen composites. Journal of materials science, 26, 5618-5622.

Phan, T. M., Park, D. W., and Le, T. H. M. (2018). Crack healing performance of hot mix asphalt containing steel slag by microwaves heating. Construction and Building Materials, 180, 503-511.

Polyethylene Terephthalate Market Analysis, Size and Trends Global Forecast To 2022–2030. (2022, April). The Business Research Company. Retrieved July 18, 2022, from https://www.thebusinessresearchcompany.com/report/polyethylene-terephthalate-global-market-report

Polyethylene Terephthalate Market Analysis, Size and Trends Global Forecast To 2022–2030. (2022, April). The Business Research Company. Retrieved July 18, 2022, from https://www.thebusinessresearchcompany.com/report/polyethylene-terephthalate-global-market-report.

Putman, B. J., and Amirkhanian, S. N. (2004). Utilization of waste fibers in stone matrix asphalt mixtures. Resources, conservation and recycling, 42(3), 265-274.

Ramakrishnan, R., Ramakrishnan, P., Ranganathan, B., Tan, C., Sridhar, T. M., and Gimbun, J. (2019). Effect of humidity on formation of electrospun polycaprolactone nanofiber embedded with curcumin using needdleless electrospinning. Materials Today: Proceedings, 19, 1241-1246.

Rosen, B. (Ed.). (1964). Fracture processes in polymeric solids: phenomena and theory. Interscience Publishers.

Sangiorgi, C., Tataranni, P., Simone, A., Vignali, V., Lantieri, C., and Dondi, G. (2016). Assessment of waste bleaching clay as alternative filler for the production of porous asphalts. Construction and Building Materials, 109, 1-7.

Santoro, M., Shah, S. R., Walker, J. L., and Mikos, A. G. (2016). Poly (lactic acid) nanofibrous scaffolds for tissue engineering. Advanced drug delivery reviews, 107, 206-212.

Schaub, N. J., Britton, T., Rajachar, R., and Gilbert, R. J. (2013). Engineered nanotopography on electrospun PLLA microfibers modifies RAW 264.7 cell response. ACS applied materials and interfaces, 5(20), 10173-10184.

Schaub, N. J., D'Amato, A. R., Mason, A., Corr, D. T., Harmon, E. Y., Lennartz, M. R., and Gilbert, R. J. (2017). The effect of engineered nanotopography of electrospun microfibers on fiber rigidity and macrophage cytokine production. Journal of Biomaterials science, Polymer edition, 28(13), 1303-1323.

Schmitt, J., and Flemming, H. C. (1998). FTIR-spectroscopy in microbial and material analysis. International biodeterioration and biodegradation, 41(1), 1-11.

Schram, S., Williams, R. C., and Buss, A. (2014). Reporting results from the Hamburg wheel tracking device. Transportation Research Record, 2446(1), 89-98.

Selvasofia, S. A., Babu, S. S., Moulica, G., Clyn, F. L., and Ram, E. S. (2022, November). A study on influence of partial replacement of bitumen by low density polyethylene. In AIP Conference Proceedings (Vol. 2446, No. 1, p. 150001). AIP Publishing LLC.

Sengoz, B., and Agar, E. (2007). Effect of asphalt film thickness on the moisture sensitivity characteristics of hot-mix asphalt. Building and environment, 42(10), 3621-3628.

Senthamizhan, A., Celebioglu, A., and Uyar, T. (2014). Flexible and highly stable electrospun nanofibrous membrane incorporating gold nanoclusters as an efficient probe for visual colorimetric detection of Hg (II). Journal of Materials Chemistry A, 2(32), 12717-12723.

Serfass, J. P., and Samanos, J. (1996). Fiber-modified asphalt concrete characteristics, applications and behavior. Asphalt Paving Technology, 65, 193-230.

Serin, S., Morova, N., Saltan, M., and Terzi, S. (2012). Investigation of usability of steel fibers in asphalt concrete mixtures. Construction and Building Materials, 36, 238-244.

Shukla, P. K., and Das, A. (2008). A re-visit to the development of fatigue and rutting equations used for asphalt pavement design. International Journal of Pavement Engineering, 9(5), 355-364.

Shukry, N. A. M., Hassan, N. A., Hainin, M. R., Abdullah, M. E., Abdullah, N. A. M., Mahmud, M. Z. H., ... and Mashros, N. (2016). Experimental evaluation of anti-stripping additives on porous asphalt mixtures. Jurnal Teknologi, 78(7-2).

Silva, J. D. A. A. E., Rodrigues, J. K. G., de Carvalho, M. W., Lucena, L. C. D. F. L., and Cavalcante, E. H. (2018). Mechanical performance of asphalt mixtures using polymer-micronized PET-modified binder. Road Materials and Pavement Design, 19(4), 1001-1009.

Simpson, A. L. (1999). Characterization of transverse profile. Transportation Research Record, 1655(1), 185-191.

Slebi-Acevedo, C. J., Lastra-González, P., Pascual-Muñoz, P., and Castro-Fresno, D. (2019). Mechanical performance of fibers in hot mix asphalt: A review. Construction and Building Materials, 200, 756-769.

Smith, R. L., Takkellapati, S., and Riegerix, R. C. (2022). Recycling of Plastics in the United States: Plastic Material Flows and Polyethylene Terephthalate (PET)

Recycling Processes. ACS Sustainable Chemistry and Engineering, 10(6), 2084-2096.

Solaimanian, M., Harvey, J., Tahmoressi, M., and Tandon, V. (2003, February). Test methods to predict moisture sensitivity of hot-mix asphalt pavements. In Transportation research board national seminar. San Diego, California (pp. 77-110).

Sperling, L. H. (2005). Introduction to physical polymer science. John Wiley and Sons.

Spinacé, M. S., and De Paoli, M. A. (2001). Characterization of poly (ethylene terephtalate) after multiple processing cycles. Journal of Applied Polymer Science, 80(1), 20-25.

Strain, I. N., Wu, Q., Pourrahimi, A. M., Hedenqvist, M. S., Olsson, R. T., and Andersson, R. L. (2015). Electrospinning of recycled PET to generate tough mesomorphic fibre membranes for smoke filtration. Journal of Materials Chemistry A, 3(4), 1632-1640.

Sulyman, M., Haponiuk, J., and Formela, K. (2016). Utilization of recycled polyethylene terephthalate (PET) in engineering materials: A review. International Journal of Environmental Science and Development, 7(2), 100.

Sun, Y., Wu, S., Liu, Q., Li, B., Fang, H., and Ye, Q. (2016). The healing properties of asphalt mixtures suffered moisture damage. Construction and Building Materials, 127, 418-424.

Tabaković, A., O'Prey, D., McKenna, D., and Woodward, D. (2019). Microwave self-healing technology as airfield porous asphalt friction course repair and maintenance system. Case Studies in Construction Materials, 10, e00233.

Tan, S. H., Inai, R., Kotaki, M., and Ramakrishna, S. (2005). Systematic parameter study for ultra-fine fiber fabrication via electrospinning process. Polymer, 46(16), 6128-6134.

Tang, G., Gao, L., Ji, T., and Xie, J. (2017). Study on the Resistance of Raveling for Porous Asphalt Pavement. DEStech Trans. Mater. Sci. Eng.

Tanzadeh, J., and Shahrezagamasaei, R. (2017). Laboratory assessment of hybrid fiber and nano-silica on reinforced porous asphalt mixtures. Construction and Building Materials, 144, 260-270.

Tanzadeh, R., Tanzadeh, J., and Tahami, S. A. (2019). Experimental study on the effect of basalt and glass fibers on behavior of open-graded friction course asphalt modified with nano-silica. Construction and building materials, 212, 467-475.

Tapkın, S. (2008). The effect of polypropylene fibers on asphalt performance. Building and environment, 43(6), 1065-1071.

The Association of Plastic Recyclers (APR). United States National Postconsumer Plastic Bottle Recycling Report in 2018. Last online access: July 12, 2022. Available through: https://plasticsrecycling.org/images/library/2018-postconsumer-bottle-recycling-report.pdf

Thompson, C. J., Chase, G. G., Yarin, A. L., and Reneker, D. H. (2007). Effects of parameters on nanofiber diameter determined from electrospinning model. Polymer, 48(23), 6913-6922.

Veleirinho, B., Rei, M. F., and Lopes-DA-Silva, J. A. (2008). Solvent and concentration effects on the properties of electrospun poly (ethylene terephthalate) nanofiber mats. Journal of Polymer Science Part B: Polymer Physics, 46(5), 460-471.

Vo, P. P., Doan, H. N., Kinashi, K., Sakai, W., Tsutsumi, N., and Huynh, D. P. (2018). Centrifugally spun recycled PET: Processing and characterization. Polymers, 10(6), 680.

Wang, H., Zhang, C., Li, L., You, Z., and Diab, A. (2016). Characterization of low temperature crack resistance of crumb rubber modified asphalt mixtures using semi-circular bending tests. Journal of Testing and Evaluation. ASTM, doi:10.1520/JTE20150145 / Vol. 44 / No. 2

Wang, X., Gao, J. P., Zhao, Q. L., Huang, J., Mao, G. L., Wu, W., Ning, Y. N., and Ma, Z. (2013). Polymethylene-block-polystyrene copolymers: A new synthetic approach using a combination of polyhomologation and reversible addition-fragmentation chain-transfer polymerization and their microfibers and microspheres fabricated through electrospinning process. Journal of Polymer Science Part A: Polymer Chemistry, 51(13), 2892-2899.

Wang, X., Wu, R., and Zhang, L. (2019). Development and performance evaluation of epoxy asphalt concrete modified with glass fibre. Road Materials and Pavement Design, 20(3), 715-726.

Wiljanen, B. R. (2003). The pavement performance and life-cycle cost impacts of carbon fiber modified hot mix asphalt (Doctoral dissertation, Michigan Technological University).

Wu, M. M., Li, R., Zhang, Y. Z., Fan, L., Lv, Y. C., and Wei, J. M. (2015). Stabilizing and reinforcing effects of different fibers on asphalt mortar performance. Petroleum Science, 12, 189-196.

Wu, M., Li, R., Zhang, Y., Wei, J., Lv, Y., and Ding, X. (2014). Reinforcement effect of fiber and deoiled asphalt on high viscosity rubber/SBS modified asphalt mortar. Petroleum Science, 11, 454-459.

Wu, S., Ye, Q., and Li, N. (2008). Investigation of rheological and fatigue properties of asphalt mixtures containing polyester fibers. Construction and Building Materials, 22(10), 2111-2115.

Wu, S., Ye, Q., Li, N., and Yue, H. (2007). Effects of fibers on the dynamic properties of asphalt mixtures. Journal of Wuhan University of Technology-Mater. Sci. Ed., 22, 733-736.

Xiao, F., Zhao, P. W., and Amirkhanian, S. N. (2009). Fatigue behavior of rubberized asphalt concrete mixtures containing warm asphalt additives. Construction and Building Materials, 23(10), 3144-3151.

Xiong, R., Fang, J., Xu, A., Guan, B., and Liu, Z. (2015). Laboratory investigation on the brucite fiber reinforced asphalt binder and asphalt concrete. Construction and Building Materials, 83, 44-52.

Xu, Q., and Solaimanian, M. (2008). Measurement and evaluation of asphalt concrete thermal expansion and contraction. Journal of Testing and Evaluation, 36(2), 507.

Xu, Y., Wang, D., Zhang, M., Wang, H., and Wei, Q. (2017). Self-layering behavior of PET fiber deposition in melt-electrospinning process. Fibers and Polymers, 18(10), 1981-1987.

Ye, Q., Wu, S., and Li, N. (2009). Investigation of the dynamic and fatigue properties of fiber-modified asphalt mixtures. International Journal of fatigue, 31(10), 1598-1602.

Yu, J., Cong, P., and Wu, S. (2009). Laboratory investigation of the properties of asphalt modified with epoxy resin. Journal of Applied Polymer Science, 113(6), 3557-3563.

Zander, N. E., Gillan, M., and Sweetser, D. (2016). Recycled PET nanofibers for water filtration applications. Materials, 9(4), 247.

Zhang, C., Li, Y., Wang, W., Zhan, N., Xiao, N., Wang, S., Li, Y., and Yang, Q. (2011). A novel two-nozzle electrospinning process for preparing microfiber reinforced pH-sensitive nano-membrane with enhanced mechanical property. European polymer journal, 47(12), 2228-2233.

Zhang, H., Li, H., Zhang, Y., Wang, D., Harvey, J., and Wang, H. (2018). Performance enhancement of porous asphalt pavement using red mud as alternative filler. Construction and building materials, 160, 707-713.

Zhang, J., and Seeger, S. (2011). Polyester materials with superwetting silicone nanofilaments for oil/water separation and selective oil absorption. Advanced Functional Materials, 21(24), 4699-4704.

Zhang, J., Guo, C., Chen, T., Zhang, W., Yao, K., Fan, C., ... and Yao, Z. (2021). Evaluation on the mechanical performance of recycled asphalt mixtures incorporated with high percentage of RAP and self-developed rejuvenators. Construction and Building Materials, 269, 121337.

Zhang, J., Huang, W., Zhang, Y., Lv, Q., and Yan, C. (2020). Evaluating four typical fibers used for OGFC mixture modification regarding drainage, raveling, rutting and fatigue resistance. Construction and Building Materials, 253, 119131.

Zhang, M., Hao, P., Dong, S., Li, Y., and Yuan, G. (2020). Asphalt binder micro-characterization and testing approaches: A review. Measurement, 151, 107255.

Zhang, W., Chen, X., Shen, S., Mohammad, L. N., Cui, B., Wu, S., and Raza Khan, A. (2021). Investigation of field rut depth of asphalt pavements using hamburg wheel tracking test. Journal of Transportation Engineering, Part B: Pavements, 147(1), 04020091.

Zhu, Y., Li, Y., Si, C., Shi, X., Qiao, Y., and Li, H. (2020). Laboratory evaluation on performance of fiber-modified asphalt mixtures containing high percentage of RAP. Advances in Civil Engineering, 2020, 1-9.

Zong, X., Kim, K., Fang, D., Ran, S., Hsiao, B. S., and Chu, B. (2002). Structure and process relationship of electrospun bioabsorbable nanofiber membranes. polymer, 43(16), 4403-4412.

2018 United States National Postconsumer Plastic Bottle Recycling Report. (2019b). In *plasticsrecycling.org*. American Chemistry Council and Association of Plastic Recyclers. Retrieved July 12, 2022, from https://plasticsrecycling.org/images/library/2018-postconsumer-bottle-recycling-report.pdf.